UPPSALA
UNIVERSITET

Digital Comprehensive Summaries of Uppsala Dissertations from the Faculty of Science and Technology 1750

Ion dynamics and structure of collisionless shocks in space

ANDREAS JOHLANDER

ACTA
UNIVERSITATIS
UPSALIENSIS
UPPSALA
2019

ISSN 1651-6214
ISBN 978-91-513-0519-6
urn:nbn:se:uu:diva-368091

Dissertation presented at Uppsala University to be publicly examined in Häggsalen, Ångströmlaboratoriet, Lägerhyddsvägen 1, Uppsala, Friday, 1 February 2019 at 13:00 for the degree of Doctor of Philosophy. The examination will be conducted in English. Faculty examiner: Professor Robert F. Wimmer-Schweingruber (Kiel University).

Abstract
Johlander, A. 2019. Ion dynamics and structure of collisionless shocks in space. *Digital Comprehensive Summaries of Uppsala Dissertations from the Faculty of Science and Technology* 1750. 63 pp. Uppsala: Acta Universitatis Upsaliensis. ISBN 978-91-513-0519-6.

Shock waves form when supersonic flows encounter an obstacle. Like in regular gases, shock waves can form in a plasma - a gas of electrically charged particles. Shock waves in plasmas where collisions between particles are very rare are referred to as collisionless shock waves. Collisionless shocks are some of the most energetic plasma phenomena in the universe. They are found for example around exploded supernova remnants and in our solar system where the supersonic solar wind encounters obstacles like planets and the interstellar medium. Shock waves in plasmas are very efficient particle accelerators though a process known as diffusive shock acceleration. An example of particles accelerated in shock waves are the extremely energetic galactic cosmic rays that permeate the galaxy. This thesis addresses the physics of collisionless shocks using spacecraft observations of the Earth's bow shock, particularly understanding the ion dynamics and shock structure for different shock conditions. For this we have used data from ESA's four Cluster satellites and NASA's four Magnetospheric Multiscale (MMS) satellites. The first study presents Cluster measurements from the quasi-parallel bow shock, where the angle between the magnetic field and the shock normal is less than 45 degrees. We study the first steps of acceleration of solar wind ions at short large-amplitude magnetic structures (SLAMS). We observe nearly specularly reflected solar wind ions upstream of a SLAMS. By gyration in the solar wind, the reflected ions are accelerated to a few times the solar wind energy. The second and third study are about shock non-stationarity using MMS measurements from the quasi-perpendicular shock, where the angle between the magnetic field and the shock normal is greater than 45 degrees. In the second study we show that the shock is non-stationary in the form of ripples that propagate along the shock surface. In the third study we study closer in detail the dispersive properties of the ripples and find that whether a solar wind ion will be reflected at the shock is dependent on where it impinges on the rippled shock. In the fourth study we quantify the conditions for ion acceleration shocks by using MMS measurements from many encounters with the bow shock. We find that the quasi-parallel shock is efficient with up to 10% of the energy density in energetic ions. We also find that at quasi-parallel shocks, SLAMS can restrict high-energy ions from propagating upstream and convect them back to the shock, potentially increasing acceleration efficiency.

Andreas Johlander, Department of Physics and Astronomy, Space Plasma Physics, 516, Uppsala University, SE-751 20 Uppsala, Sweden. Swedish Institute of Space Physics, Uppsala Division, Box 537, Uppsala University, SE-75121 Uppsala, Sweden.

ISSN 1651-6214
ISBN 978-91-513-0519-6
urn:nbn:se:uu:diva-368091 (http://urn.kb.se/resolve?urn=urn:nbn:se:uu:diva-368091)

"We're slowly coming to suspect that the space
we're traveling through is of a different kind
from what we thought whenever the word "space"
was decked out by our fantasies on Earth"
Harry Martinsson, Aniara

List of papers

This thesis is based on the following papers, which are referred to in the text by their Roman numerals.

I *Ion injection at Quasi-parallel Shocks Seen by the Cluster Spacecraft*
A. Johlander, A. Vaivads, Yu. V. Khotyaintsev, A. Retinò, and I. Dandouras
Astrophysical Journal Letters, 817:L4, 2016.
DOI: 10.3847/2041-8205/817/1/L4

II *Rippled Quasiperpendicular Shock Observed by the Magnetospheric Multiscale Spacecraft*
A. Johlander, S. J. Schwartz, A. Vaivads, Yu. V. Khotyaintsev, I. Gingell, I. B. Peng, S. Markidis, et al.
Physical Review Letters, 117:165101, 2016.
DOI: 10.1103/PhysRevLett.117.165101

III *Shock Ripples Observed by the MMS spacecraft: Ion Reflection and Dispersive Properties*
A. Johlander, A. Vaivads, Y. V. Khotyaintsev, I. Gingell, S. J. Schwartz, B. L. Giles, R. B. Torbert, and C. T. Russell
Plasma Physics and Controlled Fusion, 60(12):125006, 2018.
DOI: 10.1088/1361-6587/aae920

IV *Conditions for Ion Acceleration at Collisionless Shock Waves*
A. Johlander, A. Vaivads, Yu. V. Khotyaintsev, D. Caprioli, C. C. Haggerty, S. J. Schwartz
Manuscript in preparation

Papers not included in the thesis

Peng, I. B., Markidis, S., Laure, E., **Johlander, A.** Vaivads, A., Khotyaintsev Yu. V., Henri, P., Lapenta, G., et al. (2015), Kinetic structures of quasi-perpendicular shocks in global particle-in-cell simulations. Physics of Plasmas, 22, 092109, doi: 10.1063/1.4930212

Khotyaintsev, Y. V., Graham, D. B., Norgren, C., Eriksson, E., Li, W., **Johlander, A.**, Vaivads, A., et al. (2016), Electron jet of asymmetric reconnection, Geophys. Res. Lett., 43, 5571–5580, doi: 10.1002/2016GL069064.

Gingell, I., Schwartz, S. J., Burgess, D., **Johlander, A.**, Russell, C. T., Burch, J. L., Wilder, F. (2017). MMS observations and hybrid simulations of surface ripples at a marginally quasi-parallel shock. Journal of Geophysical Research: Space Physics, 122, 11,003–11,017. doi: 10.1002/2017JA024538 doi: 10.1002/2017JA024538

Schwartz S. J., Avanov, L., Turner, D., Zhang, H., Gingell, I., Eastwood, J. P., Gershman D.J. **Johlander A.** et al. (2018). Ion kinetics in a hot flow anomaly: MMS observations. Geophysical Research Letters. 45, 11,520–11,529. doi: 10.1029/2018GL080189

Goodrich, K. A., Ergun, R., Schwartz, S. J., Wilson, L. B. III., Newman, D., Wilder, F. D., Holmes J., **Johlander A.**, et al. (2018). MMS observations of electrostatic waves in an oblique shock crossing. Journal of Geophysical Research: Space Physics, 123. doi: 10.1029/2018JA025830

This PhD thesis is partly based on: *Ion dynamics and structure of collisionless shocks*, Licentiate dissertation, Uppsala University, A. Johlander, 2016

Contents

1. Introduction

The seemingly empty void of space between planets and stars is in fact not empty at all. Gases of free charged particles known as *plasmas* are everywhere in the universe. Plasmas are formed when electrons are stripped from neutral atoms by high-energy collisions or ionizing radiation. Many plasma environments in space can only be studied using telescopes or large computer simulations. Other plasma environments like the ones surrounding the Sun and the Earth can be reached by spacecraft specifically designed for the studies of space plasma.

Shock waves are steep and abrupt boundaries that move faster than the speed of sound and constitutes an sudden change in pressure of the material. Shock waves form when an object is placed in a supersonic flow or the object itself moves faster than the speed of sound, like supersonic aircraft or meteors entering the atmosphere. Like in ordinary gases, shock waves, or *shocks*, can form in plasmas, even when collisions between the plasma particles are very rare. Instead, energy is converted from kinetic energy of the flow to heat by the electromagnetic forces between the charged particles [Tsurutani and Stone, 1985]. These kinds of shocks are known as *collisionless shock waves*. Collisionless shocks slow down and heat up plasma and are formed for example when the supersonic *solar wind* encounters the Earth's magnetic field.

In addition to slowing down and heating plasma, collisionless shocks are also very efficient particle accelerators. Examples of shock-accelerated particles are the *cosmic rays* that permeate the galaxy. The cosmic rays are most likely produced in the gigantic shock waves that forms around supernova remnants when the ejecta from the exploded star hits the surrounding plasma [Morlino and Caprioli, 2012]. In our solar system, highly energetic ions known as *solar energetic particles* can be accelerated in shock waves following eruptions on the Sun.

Most plasma environments in the universe can only be studied remotely. This is commonly done by measuring photon emission from e.g. synchrotron radiation from electrons at the source. Such observations of collisionless shocks in astrophysical plasmas can then be interpreted using theory or numerical computer simulations. There are a class of collisionless shock waves that are accessible to study by flying spacecraft though them and take measurements of the particles and the electromagnetic fields of the plasma *in situ*. These shock waves include planetary bow shocks, interplanetary shocks, and even the solar termination shock at the edge of our solar system. The density, temperature, and magnetic field strength in solar system plasmas are quite different from the plasma at e.g. supernovas. However, the physical processes

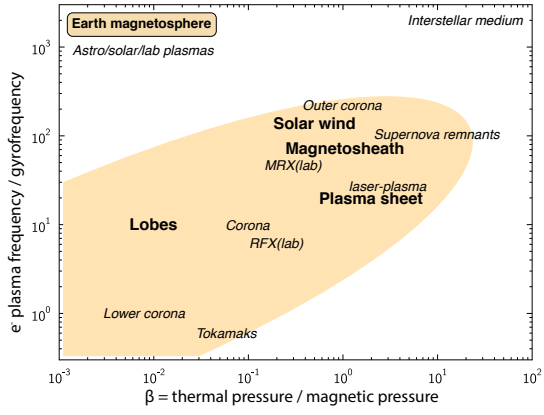

Figure 1.1. Dimensionless parameters: electron plasma frequency/cyclotron frequency, which is related to plasma density and β, which is related to temperature for different plasma environments. Diagram adapted from [Vaivads et al., 2009].

are often similar and dimensionless parameters can be rather similar, see Figure 1.1. The *in situ* measurements offer local and detailed and measurements of the plasma and can be seen as complementary to remote observations. In this thesis, we focus on *in situ* spacecraft measurements of the Earth's bow shock and use it as a natural plasma laboratory for studies of shocks. For this, we use data from ESA's Cluster and NASA's MMS multi-spacecraft missions to study shock physics specifically related to ion dynamics and shock structure for different shock conditions.

The thesis is comprised of two main parts: a comprehensive summary consisting of 9 chapters, and a collection of 4 papers where the fourth paper is a manuscript in preparation. In Chapter 2, we introduce how collisionless shocks are formed and where they are found. In Chapter 3, we focus on the Earth's bow shock and its properties. Chapter 4 is about the two spacecraft missions and the onboard scientific instruments used in this work. Chapter 5 summarizes the Rankine-Hugoniot jump conditions for shock waves that are needed for the shock-specific data analysis methods that are presented in Chapter 6. In Chapter 7 and 8 we focus on the two main topics of the papers: Chapter 7 deals with the topic of ion acceleration, and Chapter 8 is about non-stationarity and structure of shock waves. Chapter 9 is about future prospects of shock observations in space. Chapter 10 offers short summaries of the main results from the four papers.

2. Collisionless shocks

2.1 Shock waves in space

Collisionless plasmas are found in astrophysical settings such as the interstellar medium, and throughout the heliosphere in the solar wind and planetary magnetospheres. In a collisionless plasma the electric and magnetic fields play the role collisions play in neutral gases of exchanging energy between particles and propagating waves.

Like in a neutral gas, shock waves can form in collisionless plasmas [De Hoffmann and Teller, 1950]. A shock wave can form when an obstacle is placed in a fast flow. If the speed of the flow is too great for waves to propagate upstream and ”warn” the medium of the obstacle, a shock wave forms in front of the obstacle. The shock wave is a very thin transition region where the fast flow is slowed down and heated.

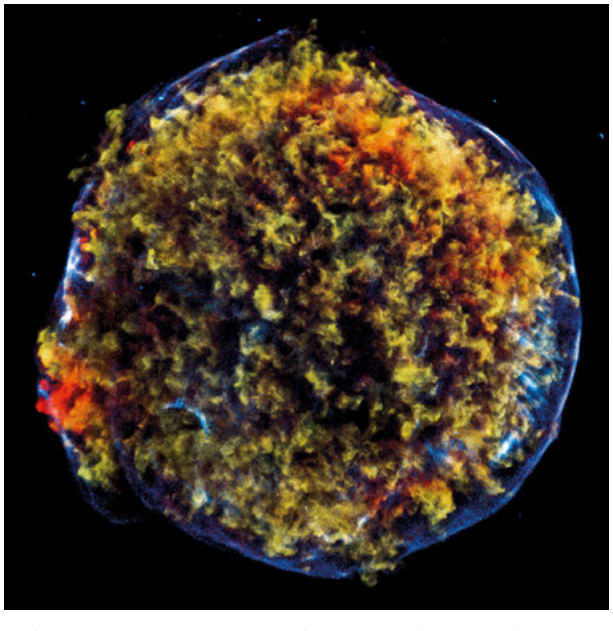

Figure 2.1. Tycho's supernova remnant in X-rays by Chandra X-ray Observatory. Image credit: NASA/CXC/SAO.

Shocks are abundant in collisionless plasmas in the universe. In the heliosphere, they form when the supersonic solar wind hits with the magnetosphere of planets, forming planetary bow shocks. A termination shock is also formed

when the solar wind is slowed before hitting the interstellar medium. When a faster portion of the solar wind overtakes a slower portion, an interplanetary shock is formed. In the solar corona, shocks are generated by solar eruptions. In astrophysical plasmas, shocks are formed for example at supernova remnants (SNRs) when the ejected material sweeps up the surrounding interstellar medium.

Collisionless shocks are efficient particle accelerators. Supernova remnant shocks are very large and energetic shocks and are most likely the source of very high energy cosmic rays. Figure 2.1 shows a supernova remnant known as Tycho's supernova in X-rays. The shock is visible as a shell around the remnant. The X-rays are due to synchrotron radiation from shock accelerated electrons [Reynolds, 2008]. There are still many open questions about the small scale structure, particle dynamics, acceleration mechanisms of shocks.

2.2 Formation

In neutral gases, a shock wave is a steepened sound wave. In collisionless plasmas, different wave modes determine the shock behavior. In magnetohydrodynamics (MHD) - a fluid plasma description - three type of waves can propagate [Swanson, 2003]. These three waves are the *slow* or sound wave, the *intermediate* or Alfvén wave, and the *fast* or magnetosonic wave. The speed of propagation of the slow wave is

$$c_s^2 = \frac{\gamma_e k_B T_e + \gamma_i k_B T_i}{m_i}, \tag{2.1}$$

where m_i is the ion mass, T_e and T_i are electron and ion temperatures respectively, and γ is specific heat. The speed of the Alfvén wave is

$$v_A = \frac{B}{\sqrt{\mu_0 N m_i}}, \tag{2.2}$$

where B is the magnetic field magnitude in the plasma and N is the plasma number density. The speed of the fast magnetosonic wave is

$$v_{ms}^2(\theta) = \frac{v_A^2 + c_s^2}{2} \pm \sqrt{\frac{(v_A^2 + c_s^2)^2}{4} - v_A^2 c_s^2 \cos^2\theta}, \tag{2.3}$$

where θ is the angle between the magnetic field and wave vector $\mathbf{k}$.

A shock wave can in principle form when a flow exceeding the group speed of any of these waves. However, the magnetosonic wave is the only MHD wave that can propagate perpendicular to the magnetic field and is always the fastest of the three. This means that most shock waves observed in space plasmas are *fast mode shocks*. Planetary bow shocks, the Sun's termination shock, and supernova remnant shocks are all fast mode shocks. These shocks

can form when upstream flow speed V_u exceeds the magnetosonic speed, i.e. the *magnetosonic Mach number*

$$M_{ms} = \frac{V_u}{v_{ms}} > 1. \tag{2.4}$$

On the downstream side of the shock, after the plasma has gone through the shock transition, the Mach number is naturally lower than one. Fast mode shocks are characterized by an increase in B, an increase N, and a decrease in V. This is illustrated in Figure 2.2 that shows MMS spacecraft measurements of an encounter with the Earth's bow shock.

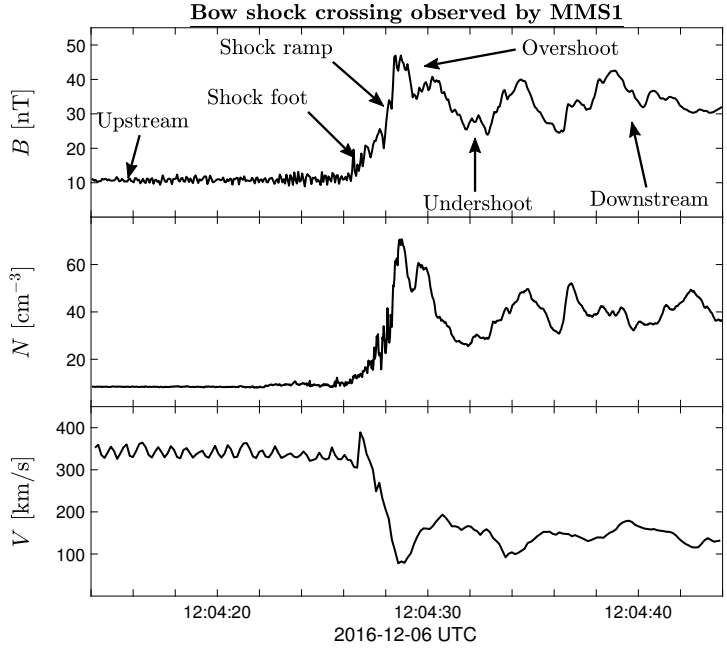

Figure 2.2. An example of MMS crossing the quasi-perpendicular bow shock. (a) Magnetic field magnitude. The different regions of the shock are marked. (b) Electron number density. (c) Ion flow speed.

2.3 Ion reflection

For a shock with M_{ms} greater than the *first critical Mach number*, the shock is unable to slow down the flow by dissipation alone [Edmiston and Kennel, 1984]. Such a *supercritical shock* is then forced to reflect a portion of the incoming upstream ions back upstream. This lowers the inflow momentum and energy density.

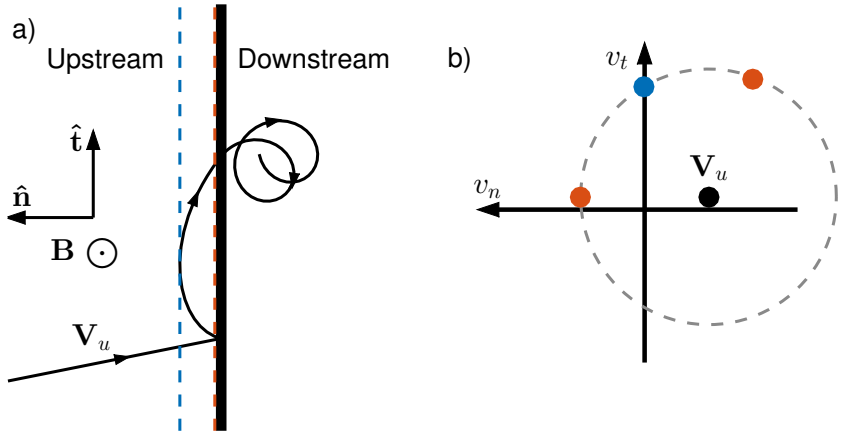

Figure 2.3. Illustration of ion reflection in real and velocity space. (a) Incoming ions with velocity $\mathbf{V}_u$ are specularly reflected off a shock. The ions return to the shock after one gyration around $\mathbf{B}_u$ and penetrate downstream. (b) ion populations in velocity space. The dashed circle marks constant energy in the upstream frame. The velocities of reflected ions at two positions marked as dashed lines in (a) are shown: Red is just upstream of the shock, here there are both newly reflected ions and returning ions. Blue is the ion velocity at the turnaround distance, the ions are moving purely tangential to the shock.

What happens to reflected ions is determined by the magnetic field geometry at the shock. Figure 2.3 illustrates ion reflection off a shock where the upstream magnetic field $\mathbf{B}_u$ is perpendicular to the shock normal vector $\hat{\mathbf{n}}$. The reflection of ions is often considered to be specular, i.e. the normal component of the velocity changes sign but the tangential velocity of the ion is conserved [Paschmann et al., 1980]. After the reflection, the ion gyrates around $\mathbf{B}_u$ with a guiding center motion directed downstream. This means that the ion is accelerated by the convection electric field $\mathbf{E}_u = -\mathbf{V}_u \times \mathbf{B}_u$. This is also illustrated in Figure 2.3b, that shows the same event in velocity space. The ion gyrates upstream of the shock with constant speed in the upstream frame. This is seen as a circle in velocity space with radius $2|\mathbf{V}_u \cdot \hat{\mathbf{n}}|$ centered around $\mathbf{V}_u$. When the ion returns to the shock the ion has a few times the energy of upstream ions. This allows the ion to penetrate the shock an pass downstream. Upstream of the shock, the reflected ions give rise to the *shock foot* and the gyrating reflected ions returning to the shock gives rise to the *overshoot* and *undershoot* in the shock, see Figure 2.2. Once the reflected ions have passed downstream they contributes to the rapid heating of the plasma.

2.4 Shock angle

Previously, we considered ions reflecting off a perpendicular shock. We now define an angle θ_{Bn} to be the acute angle between $\mathbf{B}_u$ and $\hat{\mathbf{n}}$. In the case of a perpendicular shock $\theta_{Bn} = 90°$, and for a parallel shock $\theta_{Bn} = 0°$. A shock with $\theta_{Bn} > 45°$ is referred to as *quasi-perpendicular* and a shock with $\theta_{Bn} < 45°$ as *quasi-parallel*.

The physical processes and properties of supercritical shocks is largely determined by θ_{Bn}. In the case of quasi-parallel shocks, the reflected ions do not turn around but follow the magnetic field lines back upstream where the excite various instabilities. This creates an extended foreshock region with highly developed turbulence and upstream structures. The transition from upstream to downstream in quasi-parallel shocks is very extended and happens in several steps [Schwartz and Burgess, 1991]. Quasi-perpendicular shocks are on the other hand much sharper and well-defined transitions between up- and downstream. The reflection of ions is thus the main reason for the very different characteristics of quasi-parallel and quasi-perpendicular shocks.

3. The Earth's bow shock

The Sun constantly emits a stream of plasma in all directions - this is known as the *solar wind*. The solar wind is slowed down when it encounters the magnetospheres of planets such as the Earth. Since the flow is super-magnetosonic, a blunt bow shock forms upstream of the magnetosphere. In the case of the Earth, the bow shock typically stands $\sim 15\,R_E$ upstream of the Earth, where R_E is the average radius of the Earth (6371.2 km). Since the Sun is rotating and the magnetic field is frozen-in to the plasma, the magnetic field in the solar wind often forms a spiral known as the Parker spiral [Parker, 1958]. Under these conditions, the interplanetary magnetic field at Earth is $\sim 45^\circ$ from the Earth-Sun line. This means that the dusk side of the bow shock is usually quasi-perpendicular while the dawn side is normally quasi-parallel. This is illustrated in Figure 3.1, which also highlights the difference between the turbulent and extended quasi-parallel shock and the relatively sharp quasi-perpendicular shock.

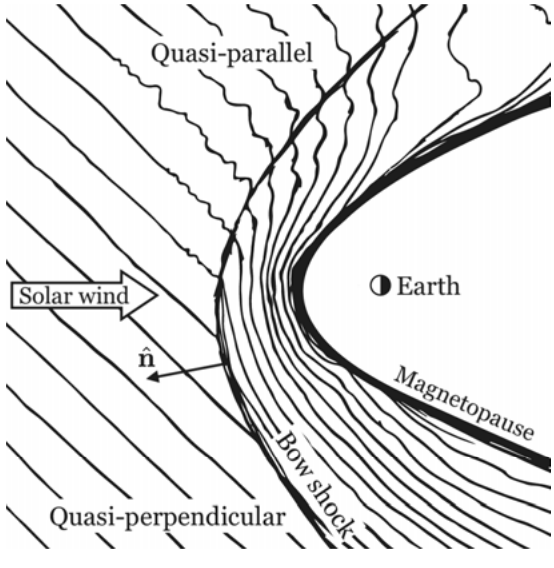

Figure 3.1. Sketch of the solar wind magnetic field lines at Earth's bow shock under Parker spiral conditions. The quasi-parallel and quasi-perpendicular sides of the bow shock are marked. The magnetosphere field lines are not shown.

The Earth's bow shock is a shock wave with varying geometry and plasma parameters. The solar wind parameters vary significantly but typical parameters are speeds of 300-700 km/s, magnetic field strength of 3-15 nT, number

density of 3-15 cm^{-3}, and ion temperature of 1-15 eV. This results in the dimensionless parameters shown in Figure 3.2. These data are compiled from the OMNI database [King and Papitashvili, 2005] and are measured by a set of spacecraft positioned upstream of the Earth at Lagrange point 1. As we can see in Figure 3.2, typical Alfvén Mach numbers of the Earth's bow shock are 5-15. These are low values compared to $M_A \sim 1000$ at SNR shocks [Reynolds, 2008]. Despite this, the Earth's bow shock share many similarities to astrophysical shocks and is an excellent laboratory where models about shocks can be tested with in situ spacecraft measurements.

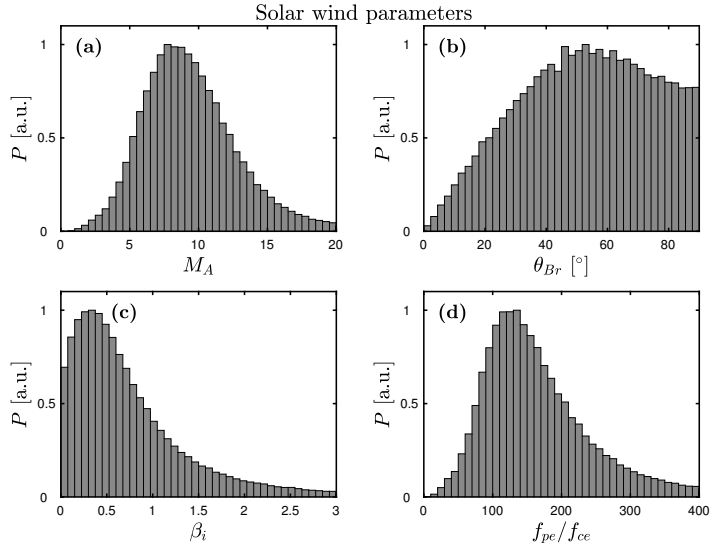

Figure 3.2. Parameters at the sub-solar point of the Earth's bow shock. Compiled from the OMNI database in the period 1995-2018. (a) Alfvén Mach number M_A. (b) Angle between solar wind magnetic field and radial direction θ_{Br}, corresponds to θ_{Bn} at the sub-solar point. (c) Upstream ion beta β_i. (d) electron plasma-to-cyclotron frequency ratio f_{pe}/f_{ce}. OMNI: `http://omniweb.gsfc.nasa.gov`.

4. Spacecraft missions and instruments

4.1 Cluster

Cluster is a European space mission to study Earth's plasma environment launched in 2000. The mission consists of four satellites flying in a tetrahedral formation with varying separation of a few km to several R_E. The satellites were launched into a highly elliptical polar orbit with a perigee of $\sim 3\,R_E$ and an apogee of $19\,R_E$. With this orbit, Cluster can perform in situ studies in various regions like the solar wind, the bow shock, the magnetopause, the polar cusps and the magnetotail. Each Cluster satellite has a cylindrical shape, 2.9 m in diameter and 1.3 m in height. Each spacecraft is rotating along the symmetry axis of the cylinder with a spin period of 4 seconds [Escoubet et al., 1997]. Cluster carries several instruments to measure various plasma parameters such as electric field, magnetic field and particle distributions of ions and electrons.

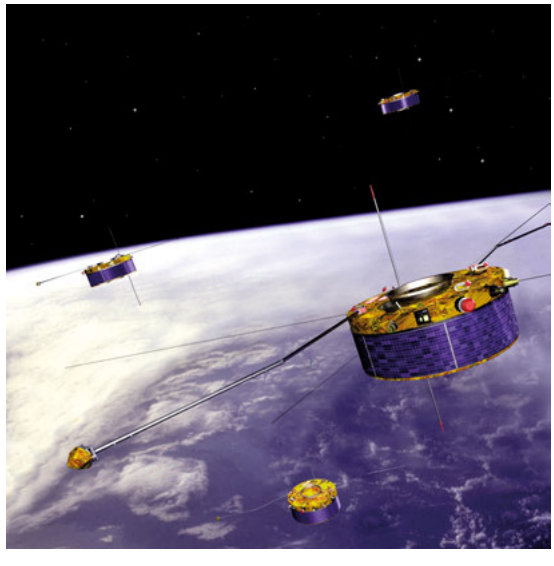

Figure 4.1. Artist's rendition of the Cluster spacecraft. Credit: ESA.

4.1.1 Cluster Ion Spectroscopy (CIS)

HIA is an ion energy spectrometer onboard Cluster measuring the ion distribution function in the different plasma regions surrounding Earth [Rème et al.,

2001]. CIS consists of two parts: the ion Composition and Distribution Function Analyser (CODIF) and the Hot Ion Analyser (HIA), where HIA is used in this work. CIS-HIA in turn consists of two sensors with different sensitivities. The sensors are mounted on the side on the spinning spacecraft and samples the ion distribution function in slices with 180° coverage in the polar direction. The instrument then relies on the spacecraft spin to sample several slices of the ion distribution function in different directions to get coverage of the full sky. Therefore, the instrument provides full three-dimensional ion distribution functions once per spin (every 4 s). In Paper I, in order to improve the time-resolution, we make use of the sub-spin resolution data from CIS-HIA using two closely-spaced Cluster spacecraft.

4.1.2 Fluxgate Magnetometer (FGM)

The FGM instrument onboard Cluster measures the slowly varying magnetic field in the surrounding plasma [Balogh et al., 2001]. The instrument consists of two triaxial sensors, meaning that it measures the three-dimensional magnetic field vector. To prevent magnetic contamination from the spacecraft, one of the sensors is mounted at the end of a deployable, solid boom and the other one at 1.5 m inboard from the end of the boom. The instrument measures both the background DC magnetic field and the fluctuating field up to a sample rate of 67 Hz.

4.2 Magnetospheric Multiscale (MMS)

The Magnetospheric Multiscale (MMS) mission is a NASA mission launched in March 2015. Like Cluster, MMS consists of four identical spacecraft flying in a tetrahedron formation, see Figure 4.2. The main science objective of MMS is related to magnetic reconnection in plasmas [Burch et al., 2016]. For this, MMS takes measurements of electromagnetic fields and particle distribution functions at reconnection sites. The two main sites of interest are the day-side magnetopause and the night-side neutral sheet in the magnetotail. The major advantage of MMS is that the particle distributions of ions and electrons are measured at much greater rate [Pollock et al., 2016] than previous missions. This, together with the shorter inter-spacecraft separation, means that MMS is able to resolve plasma physical processes at much smaller spatial and temporal scales.

While MMS was designed with magnetic reconnection in mind, the short spacecraft separation and high-cadence plasma measurements make MMS well suited for studies of small scale physical processes at the Earth's bow shock. In order to maximize the number of magnetopause encounters, MMS was launched into an equatorial, highly elliptical orbit with apogee of $12\,R_E$. After two seasons, the apogee was raised in early 2017 to $25\,R_E$ in order to

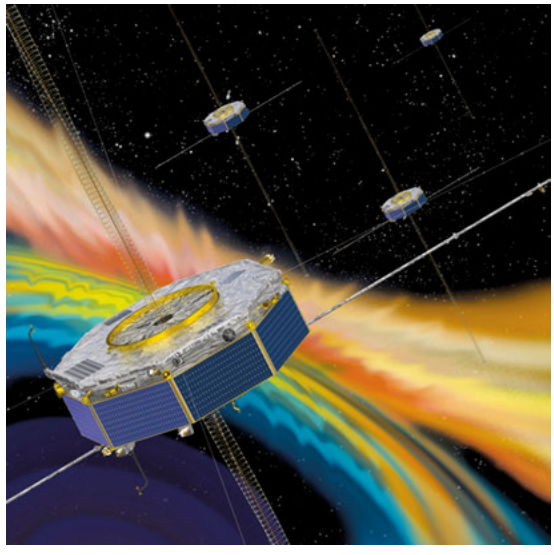

Figure 4.2. Artist's rendition of the MMS spacecraft. Credit: NASA.

study night-side reconnection in the magnetotail. Figure 4.3 shows the inter-spacecraft distances and local time at apogee for MMS from the start of the mission up until October 2018. The spacecraft separation is very small and varies between ∼5 and ∼40 km. Throughout the mission MMS has regularly encountered the bow shock, often many times per orbit due to the motion of the shock. The bow shock encounters are expected when the apogee of MMS is close to the sub-solar point, indicated by a red line in Figure 4.3. After the apogee raise, bow shock crossings are observed in a wider interval around the sub-solar point, as MMS crosses the bow shock at its flanks. All instruments onboard MMS operate in high-resolution burst mode in the region of space where reconnection events are the most likely. Only a small portion of the collected burst data can be down-linked to Earth. The data is selected for down-link by a Scientist-in-the-loop (SITL) who selects interesting interval from low-resolution data. Over the course of the mission, the SITLs have selected hundreds of bow shock encounters where burst data has been down-linked. Therefore, there is a large amount of data by MMS that is useful for studies of collisionless shock physics.

4.2.1 Fast Plasma Investigation (FPI)

The FPI instrument consists of four dual ion spectrometers (DIS) and four dual electron spectrometers (DES) [Pollock et al., 2016]. For the studies presented in this thesis, mainly data from the ion instrument FPI-DIS has been used. The energy coverage of FPI is ∼10 eV-30 keV. The FPI sensors are spread around the spacecraft body and can therefore sample the entire view of the sky

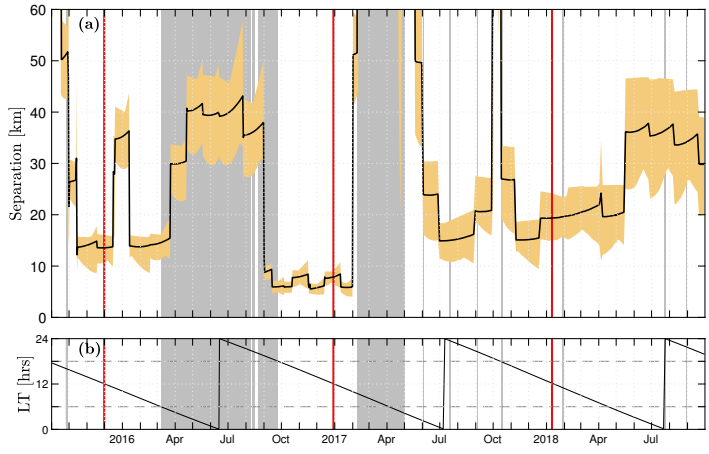

Figure 4.3. Inter-spacecraft distance and local time of apogee for the MMS spacecraft. a) Average spacecraft distance shown as a black line, orange shaded area shows min/max separation, the red vertical lines indicate where the apogee is closest to the sub-solar point, the vertical gray shade indicates where particle instruments are switched off. b) Local time of apogee, where 12 o'clock is towards the Sun.

instantaneously, and does not have to rely on the spacecraft spin. This results in that FPI can sample the plasma distribution functions much faster than any previous missions with a time resolution of 150 ms for DIS and 30 ms for DES (compare with 4 s for Cluster). This allows for measurements of plasma processes on much smaller temporal and spatial scales.

4.2.2 Fluxgate Magnetometer (FGM)

The FGM instrument onboard MMS measures the magnetic field from DC to 64 Hz [Russell et al., 2016]. The instrument consists of one analogue and one digital fluxgate magnetometer, both mounted on 5 m long deployable booms. The instrument provides the three-dimensional magnetic field vector of the surrounding plasma with a sample rate of 128 Hz. FGM is part of the FIELDS instruments suite [Torbert et al., 2016] that is dedicated to measuring the electric and magnetic field of the plasma.

4.2.3 Electric Double Probe (EDP)

The EDP instrument measures the three-dimensional electric field of the surrounding plasma. The instrument is like FGM, part of the FIELDS instrument suite. EDP consists of two sets of double-probe sensors: four spin-plane probes (SDP) that measure the electric field in the spin-plane of the spacecraft, and the two axial double probes (ADP) that measure the electric field in the

out-of-plane direction [Lindqvist et al., 2016, Ergun et al., 2016]. The SDP probes are mounted on 60 m long wire booms that are held out by the spacecraft spin and the ADP probes are mounted on 13 m long deployable solid booms that extend out of the spin plane. EPD measures the three-dimensional electric field vector down to DC with a sample rate of typically 8 kHz.

5. Rankine-Hugoniot relations

5.1 The relations

All discontinuities in plasmas, including shock waves, follow the *Rankine-Hugoniot relations*. These relations, or *jump conditions*, determine how plasma conditions on one side of the discontinuity relates to the plasma conditions on the other side. For studies of shocks in space the Rankine-Hugoniot are important since they relate the downstream plasma to the upstream plasma and is therefore useful when determining shock parameters such as shock angle and Mach numbers. The relations are six conservation laws. The Rankine-Hugoniot relations are presented below. Here, we adopt the subscripts "u" for upstream values, "d" for downstream, n for normal to the discontinuity, and t for tangential to the discontinuity. We also use the notation $[\chi] = \chi_u - \chi_d$.

First, the conservation of the mass flux over the discontinuity means that

$$[NmV_n] = 0, \tag{5.1}$$

where N is the plasma number density, m is the mass of the particles in the plasma, typically the ion mass, and $\mathbf{V}$ is the flow velocity of the plasma. Next, conservation of momentum flux normal to the discontinuity gives

$$\left[NmV_n^2 + P + \frac{B_t^2}{2\mu_0}\right] = 0. \tag{5.2}$$

where $\mathbf{B}$ is the magnetic field, and P is the thermal pressure of the plasma. Conservation of momentum flux tangential to discontinuity gives

$$\left[NmV_n\mathbf{V}_t - B_n\frac{\mathbf{B}_t}{\mu_0}\right] = 0. \tag{5.3}$$

Conservation of energy flux means that

$$\left[NmV_n\left(\frac{\gamma}{\gamma-1}\frac{P}{nm} + \frac{V^2}{2} + \frac{\mathbf{B}_t^2}{\mu_0 Nm}\right) - (\mathbf{V}_t\cdot\mathbf{B}_t)\frac{B_n}{\mu_0}\right] = 0. \tag{5.4}$$

The Maxwell equation $\nabla\cdot\mathbf{B} = 0$ gives

$$[B_n] = 0. \tag{5.5}$$

Finally, conservation of tangential electric field gives through $\mathbf{E} = -\mathbf{V}\times\mathbf{B}$

$$[B_n\mathbf{V}_t - V_n\mathbf{B}_t] = 0. \tag{5.6}$$

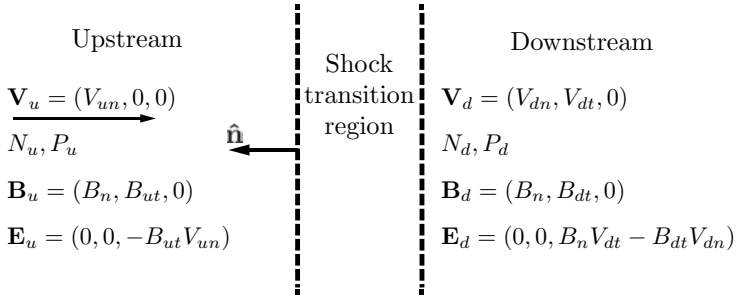

Figure 5.1. The shock wave in the NI frame with up- and downstream plasma conditions.

5.2 Shock waves

The Rankine-Hugoniot relations are valid in all frames of reference and all types of discontinuities in plasmas, not just shock waves. In order to make these relations more useful for observations of shocks in space, we need to define a reference frame. We use a frame where the shock is at rest and the incoming upstream plasma velocity is along the shock normal vector. The frame is illustrated in Figure 5.1, which shows the shock transition. Note that the Rankine-Hugoniot relations relate the asymptotic up- and downstream values; the conditions inside the shock transition region are subject to kinetic scale processes and cannot be expected to fulfill the jump conditions. The frame illustrated in Figure 5.1 is commonly used in shock physics and is referred to as the Normal Incidence (NI) frame. In the NI frame

$$\mathbf{V}_u = V_{un}\hat{\mathbf{n}}, \tag{5.7a}$$

$$\mathbf{B}_u = B_{un}\hat{\mathbf{n}} + B_{ut}\hat{\mathbf{t}}, \tag{5.7b}$$

where $\hat{\mathbf{n}}$ and $\hat{\mathbf{t}}$ are the normal and tangential unit vectors respectively. In the case of shock waves, both $\mathbf{B}$ and $\mathbf{V}$ are *coplanar*. This means that $\mathbf{B}_d$ and $\mathbf{V}_d$ will both be in the *coplanarity plane* formed by $\mathbf{B}_u$ and $\hat{\mathbf{n}}$, see Figure 5.1. Therefore there is no rotation in either the magnetic field of plasma flow velocity out of the $n-t$ plane. We get

$$\mathbf{V}_d = V_{dn}\hat{\mathbf{n}} + V_{dt}\hat{\mathbf{t}}, \tag{5.8a}$$

$$\mathbf{B}_d = B_{dn}\hat{\mathbf{n}} + B_{dt}\hat{\mathbf{t}}. \tag{5.8b}$$

Using this, the Rankine-Hugoniot relations for fast mode shock waves are listed below.

Conservation of mass flux (5.1) becomes

$$N_uV_{un} = N_dV_{dn}, \tag{5.9}$$

conservation of normal momentum flux (5.2) becomes

$$N_u m V_{un}^2 + P_u + \frac{B_{ut}^2}{2\mu_0} = N_d m V_{dn}^2 + P_d + \frac{B_{dt}^2}{2\mu_0}, \tag{5.10}$$

conservation of tangential momentum flux (5.3) becomes

$$-B_n \frac{B_{ut}}{\mu_0} = N_d m V_{dn} V_{dt} - B_n \frac{B_{dt}}{\mu_0}, \tag{5.11}$$

conservation of energy flux (5.4) becomes

$$\begin{aligned} N_u m V_{un} \left(\frac{\gamma}{\gamma - 1} \frac{P_u}{N_u m} + \frac{V_{un}^2}{2} + \frac{B_{ut}^2}{\mu_0 N_u m} \right) - \\ N_d m V_{dn} \left(\frac{\gamma}{\gamma - 1} \frac{P_d}{N_d m} + \frac{V_{dn}^2 + V_{dt}^2}{2} + \frac{B_{dt}^2}{\mu_0 N_d m} \right) + V_{dt} B_{dt} \frac{B_n}{\mu_0} = 0 \end{aligned} \tag{5.12}$$

$\nabla \cdot \mathbf{B} = 0$ (5.5) becomes

$$B_{un} = B_{dn} = B_n, \tag{5.13}$$

and conservation of tangential electric field (5.6) becomes

$$-V_{un} B_{ut} = B_n V_{dt} - V_{dn} B_{dt}, \tag{5.14}$$

where (5.13) has been implicitly used in all above expressions.

This is a set of five linear equations with five unknowns, N_d, V_{dn}, V_{dt}, B_{dt}, and P_d, given the values of N_u, V_{un}, B_n, B_{ut}, and P_u. This set of equation can be solved in order to determine the downstream plasma conditions of a shock from the upstream conditions. These relations are useful when determining e.g. the speed of a shock wave that is propagating past an observing spacecraft. Next we will solve the Rankine-Hugoniot relations in the limit of a strong wave to illustrate how the shock compresses the plasma in high-Mach-number shocks.

5.3 Strong shocks

All fast shock solutions to the Rankine-Hugoniot relations requires $M_{ms} > 1$. In the limit M_{ms}=1 only the trivial solution N_d/N_u=1 exists, i.e. the shock does not compress the plasma at all. For stronger shock waves with higher Mach numbers the plasma is compressed. However, in the limit of strong shock waves, the compression ratio N_d/N_u approaches some value. To find this value, we consider a shock wave where the upstream momentum and energy flux is dominated by the plasma bulk flow; thermal pressure magnetic tension are considered negligible. Thus, (5.10) becomes

$$P_d = N_u m V_{un}^2 - N_d m V_{dn}^2 = N_u m V_{un}^2 \left(1 - \frac{N_u}{N_d}\right), \tag{5.15}$$

where the pressure upstream is due to bulk motion of the plasma and downstream by bulk motion and thermal pressure. Inserting this into (5.12) gives

$$N_u m \frac{V_{un}^3}{2} = N_u m V_{un} \left[\frac{\gamma}{\gamma - 1}\frac{N_u}{N_d} V_{un}^2 \left(1 - \frac{N_u}{N_d}\right) + \frac{N_u^2}{N_d^2}\frac{V_{un}^2}{2}\right], \tag{5.16}$$

which simplifies to

$$\frac{1}{2}\left(1 - \frac{N_u^2}{N_d^2}\right) = \frac{\gamma}{\gamma - 1}\left(\frac{N_u}{N_d} - \frac{N_u^2}{N_d^2}\right) \tag{5.17}$$

We then get the plasma compression ratio in the limit of a strong shock wave

$$\frac{N_d}{N_u} = \frac{\gamma + 1}{\gamma - 1}. \tag{5.18}$$

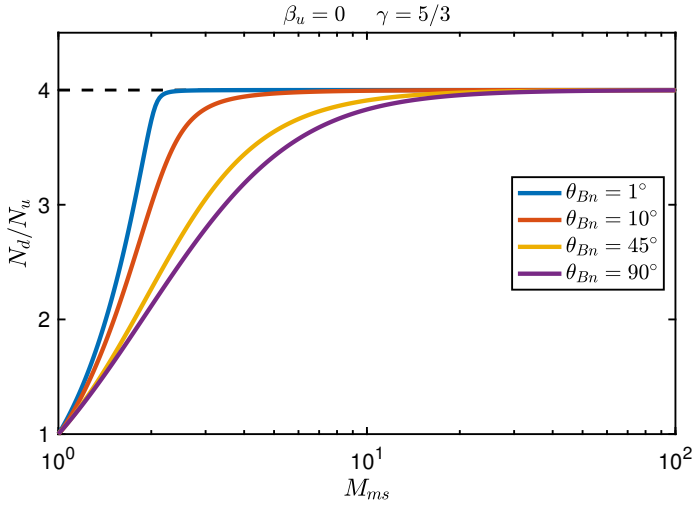

Figure 5.2. Compression ratio N_d/N_u dependence on fast magnetosonic Mach number M_{ms} for a shock wave where $\theta_{Bn} = 60°$, $\beta_u = 0$, and $\gamma = 5/3$.

In the case of a monoatomic, single species plasma, there are 3 degrees of freedom and $\gamma = 5/3$. In this case the compression ratio tends towards 4 for high-Mach-number shocks. Figure 5.2 shows semi-analytical solutions to equations (5.9-5.14) and shows the Mach number dependence of the compression ratio N_d/N_u. This result is universal for collisionless shock waves and a compression factor of 4 is often observed at the Earth's bow shock [Formisano et al., 1973].

6. Data analysis methods

In this chapter, we review some measurement techniques to determine shock parameters like normal vector, shock angle and Mach number of a shock that is observed by one or several spacecraft. See [Schwartz, 1998] for a further information and more tools.

6.1 Shock normal vector

For any analysis of shock waves in space, an accurate determination of the orientation of the shock plane and normal vector is key. Since the orientation of the shock wave is unknown, we have to use the measurements taken on the observing spacecraft. Here, we will review a few methods to determine the shock normal vector $\hat{\mathbf{n}}$. One group of techniques make use of the coplanarity of $\mathbf{B}$ and $\mathbf{V}$ and only requires measurements from a single spacecraft. Other measurements of $\hat{\mathbf{n}}$ require measurements by four or more spacecraft. In the case of the bow shock there are also empirical models of the shape and therefore normal direction of the shock. All of these methods may be useful in different scenarios.

6.1.1 Multi-spacecraft timing

When more than one spacecraft cross a shock, they will do so at different times. With information of the time of the crossing and the relative positions of the spacecraft it is possible to calculate both the direction the shock is propagating in, and its speed.

Consider four spacecraft in a tetrahedron formation, like Cluster or MMS, that observes a shock, or some other discontinuity or wave, that passes each spacecraft. The times at which the discontinuity is observed at each spacecraft are t_α where $\alpha = 1,2,3,4$. These times are picked out from measurements of e.g. magnetic field and are found either by hand or with some algorithm like minimizing the *mean square deviation* of the signals. The position in space of each spacecraft is given by $\mathbf{r}_\alpha$ at the time of the crossing t_α. Spacecraft positions are typically given in reference to the center of the Earth. The spacecraft position relative to the tetrahedron center is

$$\mathbf{r}_{*\alpha} = \mathbf{r}_\alpha - \mathbf{r}_*, \tag{6.1}$$

where

$$\mathbf{r}_* = \frac{1}{4}\sum_{\alpha=1}^{4}\mathbf{r}_\alpha. \tag{6.2}$$

Then the *position tensor* is

$$\mathbf{R}_* = \sum_{\alpha=1}^{4}\mathbf{r}_*\mathbf{r}_*^{\mathsf{T}} \tag{6.3}$$

and the generalized *reciprocal vectors* for each spacecraft are

$$\mathbf{q}_\alpha = \mathbf{R}_*^{-1}\mathbf{r}_{*\alpha}. \tag{6.4}$$

This description of the spacecraft position in reciprocal vectors makes it easier to calculate orientation and speed of the discontinuity.

The *slowness vector* of a discontinuity is defined as

$$\mathbf{m} = \frac{\hat{\mathbf{n}}}{V_{sh}}, \tag{6.5}$$

where V_{sh} is the speed of the shock or the discontinuity. The slowness vector of the discontinuity can be calculated by [Vogt et al., 2011]

$$\mathbf{m} = \sum_{\alpha=1}^{4}\mathbf{q}_\alpha t_\alpha. \tag{6.6}$$

that holds for any arbitrary time offset. t_α can therefore be for example the time difference of the observations relative to the first spacecraft. From the slowness vector we can get both the normal vector and speed of the discontinuity.

To illustrate the timing analysis method on a shock wave we consider an interplanetary shock wave observed by MMS. Figure 6.1 shows the spacecraft position and the magnetic field magnitude B observed by the four spacecraft during the shock crossing. Figure 6.1d shows the time-shifted signals $B(t-t_\alpha)$ where t_α is found by minimizing the mean square deviation of B. The resulting normal vector and speed shows that the shock wave is being convected downstream by the solar wind. In the solar wind frame however, the shock is propagating upstream. Knowing the normal and propagation speed is required to determine the parameters such as shock angle and Mach number of the shock.

6.1.2 Single-spacecraft methods

Magnetic coplanarity

For fast shock waves, the magnetic field up- and downstream are in the same plane – they are coplanar. This fact can be used to determine the orientation

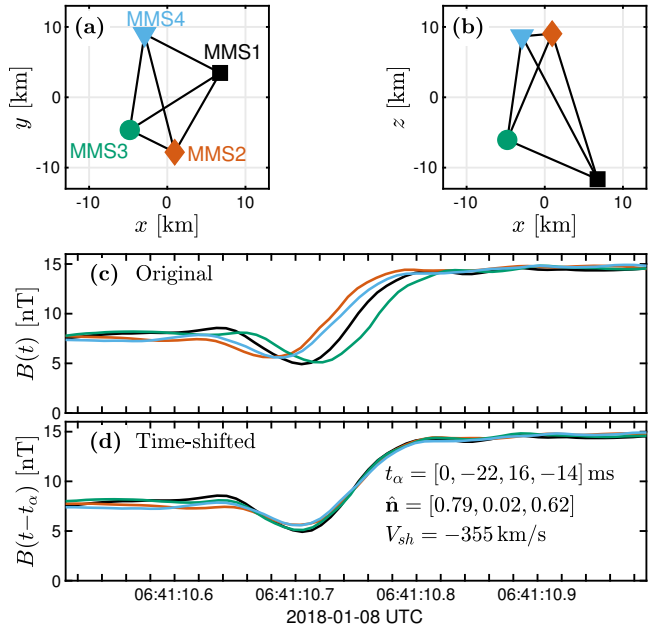

Figure 6.1. Four-spacecraft timing performed on a crossing of an interplanetary shock wave by MMS. (a-b) relative spacecraft positions $\mathbf{r}_{*\alpha}$ in GSE. (c) Magnetic field magnitude observed by all four spacecraft. (d) Time-shifted magnetic field magnitude with resulting normal vector and shock speed.

of a shock as long as the spacecraft can accurately measure the magnetic field vector. In order to determine the normal vector we need two vectors perpendicular to $\hat{\mathbf{n}}$. One such vector is $\Delta\mathbf{B} = \mathbf{B}_d - \mathbf{B}_u$ since B_n is the same on both sides of the shock. Due to the coplanarity of $\mathbf{B}$, $\mathbf{B}_d \times \mathbf{B}_u$ is also perpendicular to $\hat{\mathbf{n}}$. We can then determine the normal vector using magnetic coplanarity

$$\hat{\mathbf{n}} = \pm \frac{(\mathbf{B}_d \times \mathbf{B}_u) \times \Delta\mathbf{B}}{|(\mathbf{B}_d \times \mathbf{B}_u) \times \Delta\mathbf{B}|}. \tag{6.7}$$

One should take care when using this method to find $\hat{\mathbf{n}}$ as the method breaks down when the up- and downstream magnetic fields are nearly parallel, which happens when θ_{Bn} is close to either 0 or 90°.

Velocity coplanarity

The velocity of the plasma up- and downstream of the shock are, like the magnetic field, coplanar. However, we have no conservation law like for B_n. Instead, we can use the fact that when magnetic stresses are relatively unimportant, which happens when θ_{Bn} is close to either 0 or 90° or when the Mach number of the shock is high, the tangential velocity change is small and $|\Delta\mathbf{V}| \approx \Delta\mathbf{V} \cdot \hat{\mathbf{n}}$. Therefore, the normal can be approximated as

$$\hat{\mathbf{n}} = \pm \frac{\Delta \mathbf{V}}{|\Delta \mathbf{V}|}. \tag{6.8}$$

Mixed approach

Both the single-spacecraft methods to determine $\hat{\mathbf{n}}$ using magnetic and velocity coplanarity have weaknesses. It is possible, however, to combine measurements of the magnetic field and velocity vector to get a more robust determination of $\hat{\mathbf{n}}$. As an alternative to $\mathbf{B}_d \times \mathbf{B}_u$ as a vector perpendicular to $\hat{\mathbf{n}}$, which is unreliable when $\mathbf{B}_d$ and $\mathbf{B}_u$ are close to parallel, we can use e.g. $\Delta\mathbf{B} \times \Delta\mathbf{V}$, which should be perpendicular to $\hat{\mathbf{n}}$. We then get a *mixed mode* expression for the shock normal

$$\hat{\mathbf{n}} = \pm \frac{(\Delta\mathbf{B} \times \Delta\mathbf{V}) \times \Delta\mathbf{B}}{|(\Delta\mathbf{B} \times \Delta\mathbf{V}) \times \Delta\mathbf{B}|}. \tag{6.9}$$

The $\Delta\mathbf{B}$ can be changed to either $\mathbf{B}_d$ or $\mathbf{B}_u$ while still being as valid. These mixed mode normal estimations were first used by [Abraham-Shrauner, 1972] and are robust methods to determine $\hat{\mathbf{n}}$ under most shock conditions as long as the asymptotically up- and downstream plasma parameters can be accurately determined.

6.1.3 Bow shock models

In the case of the Earth's bow shock, there are a number empirical models of the shape of the bow shock. The bow shock models are typically conic sections [Schwartz, 1998] and are in the form

$$\frac{L}{r'} = 1 + \varepsilon \cos\theta', \tag{6.10}$$

where the primed symbols mark that the coordinate system offset from the center of the Earth and rotated off the Sun-Earth line due to the orbital motion of the Earth. The different models have different parameters for the length scale L, ellipticity ε, and how to convert to the primed coordinate system.

The bow shock models can be scaled with the dynamic pressure of the solar wind. In reality, the bow shock location varies a lot more than this scaling. When dealing with spacecraft data from the bow shock the location of the bow shock is known. It is therefore possible to force the bow shock model to fit through the spacecraft location to get an estimate of $\hat{\mathbf{n}}$. There are several different empirical models of the bow shock, see [Schwartz, 1998]. A few of them are illustrated in Figure 6.2 that shows the models forced through the position of an imagined spacecraft. With the bow shock models it is possible to get a good estimate of shock normal even when the plasma measurements are difficult to interpret.

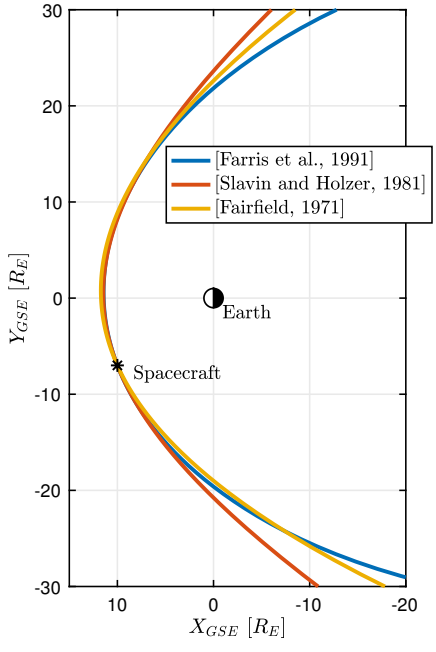

Figure 6.2. Bow shock models forced through the position of an imagined spacecraft that is located at $\mathbf{R} = (10, -7, 0)R_E$. In GSE coordinates. The three bow shock models are shown as colored lines.

6.2 The normal incidence frame

In the following two sections about shock speed and Mach numbers, we will rely on the normal incidence (NI) frame. Since shock waves in space are moving relative to the observing spacecraft it is useful to convert between the spacecraft frame and the NI frame. Unprimed parameters are in the spacecraft frame and primed parameters are in the NI frame. Since we're dealing with non-relativistic shock waves the magnetic field $\mathbf{B}$ is the same in both frames. We use the frame transformation

$$\mathbf{V}' = \mathbf{V} - \mathbf{V}_{NIF}. \tag{6.11}$$

where the primed $\mathbf{V}'$ is the plasma flow in the NI frame and $\mathbf{V}_{NIF}$ is the velocity of the NI frame in the spacecraft frame. In the NI frame, the upstream flow is along $\hat{\mathbf{n}}$ and the shock is stationary. Therefore

$$\mathbf{V}_{NIF} = \mathbf{V}_{ut} + V_{sh}\hat{\mathbf{n}}, \tag{6.12}$$

where $\mathbf{V}_{ut}$ is the upstream tangential flow velocity and V_{sh} is the speed of the shock wave in the spacecraft frame. This can also be expressed as

$$\mathbf{V}_{NIF} = \mathbf{V}_u - (\mathbf{V}_u \cdot \hat{\mathbf{n}} - V_{sh})\hat{\mathbf{n}}. \tag{6.13}$$

6.3 Shock speed

Four-spacecraft timing analysis provides not only the normal vector, but also the speed of a discontinuity that passes the spacecraft. There are cases when timing analysis is not an option because the spacecraft see shock profiles that are too different to establish time differences, or for MMS, that the spacecraft are too closely spaced that the spacecraft essentially see the shock at the same time. There are then single spacecraft methods that rely either on one of the frame-dependent Rankine-Hugoniot relations or the presence of shock reflected ions.

6.3.1 Mass flux

In the case of a uniform and stationary shock the mass flux should be the same on both sides of the shock wave. In the spacecraft frame the shock is not stationary however, so if we have reliable measurements of plasma density, flow velocity, and $\hat{\mathbf{n}}$ we can estimate the shock speed in the spacecraft frame V_{sh}. Transforming the mass flux conservation law (5.9) to the spacecraft frame, we get

$$N_u(\mathbf{V}_u \cdot \hat{\mathbf{n}} - V_{sh}) = N_d(\mathbf{V}_d \cdot \hat{\mathbf{n}} - V_{sh}). \tag{6.14}$$

Solving for the shock speed in the spacecraft frame, we get

$$V_{sh} = \frac{(N_d\mathbf{V}_d - N_u\mathbf{V}_u) \cdot \hat{\mathbf{n}}}{N_d - N_u}. \tag{6.15}$$

6.3.2 Tangential electric field

A method to determine shock speeds proposed by [Smith and Burton, 1988] takes use of the conservation of the tangential electric field using measurements of the magnetic field and plasma flow velocity. The tangential electric field conservation (5.14) becomes in the spacecraft frame

$$(\mathbf{V}_u \cdot \hat{\mathbf{n}} - V_{sh})\hat{\mathbf{n}} \times \mathbf{B}_u = [\mathbf{V}_d - \mathbf{V}_u + (\mathbf{V}_u \cdot \hat{\mathbf{n}} - V_{sh})\hat{\mathbf{n}}] \times \mathbf{B}_d, \tag{6.16}$$

which becomes

$$|\mathbf{V}_u \cdot \hat{\mathbf{n}} - V_{sh}| = \frac{|(\mathbf{V}_d - \mathbf{V}_u) \times \mathbf{B}_d|}{|\mathbf{B}_d - \mathbf{B}_u|}. \tag{6.17}$$

Since $\hat{\mathbf{n}}$ points upstream, $\mathbf{V}_u \cdot \hat{\mathbf{n}} < 0$ and we know that $|V_{sh}| < |\mathbf{V}_u \cdot \hat{\mathbf{n}}|$, we get that

$$V_{sh} = \mathbf{V}_u \cdot \hat{\mathbf{n}} + \frac{|(\mathbf{V}_d - \mathbf{V}_u) \times \mathbf{B}_d|}{|\mathbf{B}_d - \mathbf{B}_u|}. \tag{6.18}$$

It is possible to derive an expressions for V_{sh} from all frame-dependent Rankine-Hugoniot relations but measurement limitations of in particular the plasma thermal pressure in the upstream solar wind can make these methods unreliable.

6.3.3 Shock foot thickness

Above a certain Mach number, collisionless shock waves start to reflect ions. It is often assumed that the reflection is specular. Schwartz et al. [1983] derived the trajectories of these reflected ions. Since the shock foot is caused by the reflected ions, if we know the maximum distance from the shock the reflected ions are expected to reach and for how long we observe the shock foot, we can derive the speed at which the shock is traveling. Gosling and Thomsen [1985] derived the relation

$$V_{sh} = \frac{d}{\Delta t} = \mathbf{V}_u \cdot \hat{\mathbf{n}} \left(\frac{x_o}{1 \pm x_o} \right) \tag{6.19}$$

where d is the distance where the reflected ions turn back toward the shock, Δt is the time duration of the shock foot, and

$$x_o = \frac{f(\theta_{Bn})}{\omega_{ci} \Delta t} \tag{6.20}$$

where ω_{ci} is the ion cyclotron frequency and the unitless function $f(\theta_{Bn})$ is

$$f(\theta_{Bn}) = \omega_{ci} t_1 (2\cos^2 \theta_{Bn} - 1) + 2\sin^2 \theta_{Bn} \sin \omega_{ci} t_1 \tag{6.21}$$

where t_1 is the time required for reflected ions to turn around and fulfills

$$\cos \omega_{ci} t_1 = \frac{1 - 2\cos^2 \theta_{Bn}}{2\sin^2 \theta_{Bn}}. \tag{6.22}$$

With this method it is possible to find the speed of quasi-perpendicular shocks where a clear shock foot can be observed. The shock foot duration must be picked out by hand and can therefore be somewhat uncertain.

6.4 Comparison of methods

Here, we study one example of a bow shock crossing observed by all four Cluster satellites on 2001-02-20. Figure 6.3 shows data from the shock crossing. We use different methods to determine the normal vector and speed of the shock.

Starting with timing analysis, we find that the local normal vector of the bow shock is $\hat{\mathbf{n}} = (0.93, -0.21, -0.29)$, which means that this is a quasi-perpendicular shock with $\theta_{Bn} = 63^\circ$. We also find that $V_{sh} = 28\,\text{km/s}$. In

this case $\hat{\mathbf{n}}$ points upstream and $V_{sh} > 0$, which means that the shock is moving upstream, which we already knew since the spacecraft go from upstream to downstream. Here, the shock profile seen by the four spacecraft are rather similar and clearly separated in time, this means that timing analysis is probably rather reliable.

We then calculate the normal and speed of the shock using the various single-spacecraft methods listed above. To find the up- and downstream parameters we average the spacecraft measurements in the time intervals indicated in Figure 6.3. Due to the larger fluctuations downstream, it is usually a good idea to select a long time interval there. The plasma parameters up- and downstream are listed in Table 6.1. The shock crossing appears to be stable with no sudden changes in the solar wind, so we expect the single spacecraft methods to be reliable.

Table 6.1. *Up- and downstream measured by Cluster for the shock crossing in Figure 6.3.*

Parameter	Value
$\mathbf{B}_u$	$(6.7, -3.9, 7.4)$ nT
$\mathbf{B}_d$	$(9.9, -11.1, 25.7)$ nT
N_u	$4.4\,\mathrm{cm}^{-3}$
N_d	$36.3\,\mathrm{cm}^{-3}$
$\mathbf{V}_u$	$(-327, 48, -15)$ km/s
$\mathbf{V}_d$	$(-111, 28, -99)$ km/s

The resulting normals and speeds are listed in Table 6.2. All shock normals are rather close to the timing analysis. The worst is the bow shock model normal that is 10° from the timing and the best is the mixed mode normal at 6° from the timing. These deviations can be seen as a rough estimate of uncertainty of the normal determination.

We also calculate the speed of the shock using the single-spacecraft methods described above. The results are listed in Table 6.2. For the shock foot thickness by Gosling and Thomsen [1985], we estimate the shock foot to be observed for 10 s. The resulting V_{sh} is very close to the timing results. The method using conservation of tangential electric field also produces a result that is reasonably close to the timing analysis. The mass flux method, however, is very far from the other methods and even gives the wrong sign of V_{sh}. The reason for this is most likely that the ion instrument CIS-HIA onboard Cluster underestimates the plasma number density in the cold and fast solar wind. We can also see this in the compression factor N_d/N_u that is $\sim$8, which we know from the Rankine-Hugoniot is not allowed (see Section 5.3). This is also supported by the solar wind monitor spacecraft *ACE* which is positioned upstream of Cluster and measures $N_u = 9\,\mathrm{cm}^{-3}$. This highlights one of the

considerations regarding accuracy and reliability of methods when working with spacecraft data from shocks in space.

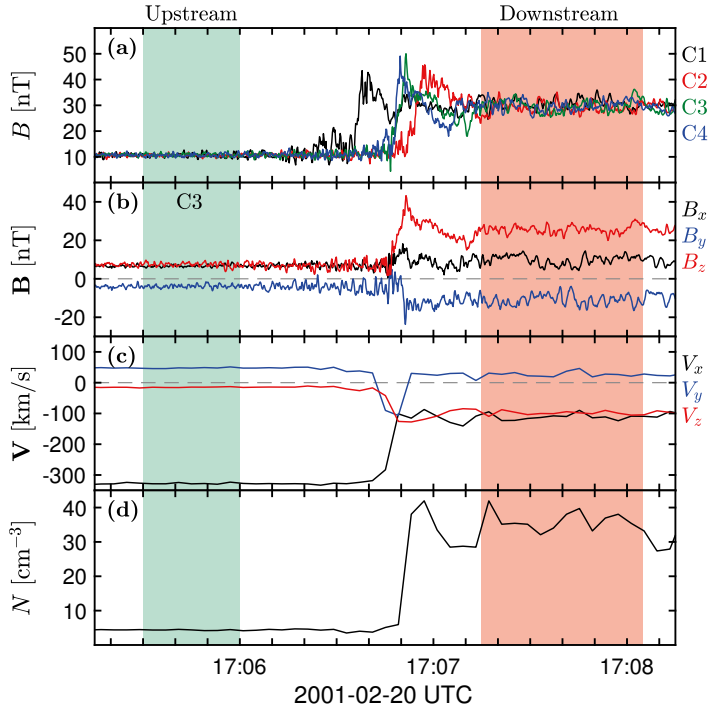

Figure 6.3. Shock crossing by the Cluster spacecraft used to illustrate the different analysis methods. The up- and downstream intervals used are indicated by the shaded areas. (a) magnetic field magnitude for all four spacecraft. (b) magnetic field measured by C3 in GSE. (c) Ion bulk velocity. (d) Ion number density.

Table 6.2. *Resulting normal vectors* $\hat{\mathbf{n}}$ *and shock speed for different methods.*

Normal vectors		**Speeds**	
Timing	(0.93, -0.21, -0.29)	Timing	28 km/s
B coplanarity	(0.97, -0.10, -0.21)	Mass flux	-49 km/s
V coplanarity	(0.93, -0.09, -0.36)	Tangential **E**	36 km/s
Mixed mode	(0.96, -0.14, -0.22)	Shock foot th.	25 km/s
Bow shock model[a]	(0.97, -0.06, -0.23)		

[a] Model by [Farris et al., 1991].

6.5 Mach numbers

In collisionless shock physics, the term *Mach number* can be ambiguous. In MHD there are three wave modes: the slow (sonic), the intermediate (Alfvén)

and fast (magnetosonic) wave mode. Mach numbers are the upstream flow speed divided by group speed of any of these three wave modes. The two most commonly used Mach numbers are the *Alfvén Mach number* and the *magnetosonic Mach number*, which are defined in slightly different ways. We will here go through how to calculate these Mach numbers from spacecraft data.

The Alfvén speed in a plasma is given by

$$v_A = \frac{B}{\sqrt{\mu_0 N m_i}}, \tag{6.23}$$

where m_i is the ion mass. The sound speed in a plasma is given by [Chen and von Goeler, 1985]

$$c_s^2 = \frac{\gamma_e k_B T_e + \gamma_i k_B T_i}{m_i}, \tag{6.24}$$

where T_i and T_e are the ion and electron temperatures respectively and the specific heats $\gamma_e = 1$ and $\gamma_i = 3$. The group speed of a magnetosonic wave for an arbitrary propagation angle θ to $\mathbf{B}$ is given by [Swanson, 2003]

$$v_{ms}^2(\theta) = \frac{v_A^2 + c_s^2}{2} + \sqrt{\frac{(v_A^2 + c_s^2)^2}{4} - v_A^2 c_s^2 \cos^2\theta}. \tag{6.25}$$

In section 6.2 we defined the coordinate transformation from the spacecraft frame to the NI frame. The NI frame is a physically relevant frame when calculating Mach numbers. We see that specifically the upstream velocity in the NI frame is

$$\mathbf{V}_u' = (\mathbf{V}_u \cdot \hat{\mathbf{n}} - V_{sh})\hat{\mathbf{n}}. \tag{6.26}$$

Now, the magnetosonic Mach number in the NI frame is

$$M_{ms} = \frac{|\mathbf{V}_u \cdot \hat{\mathbf{n}} - V_{sh}|}{v_{ms}(\theta_{Bn})}, \tag{6.27}$$

where θ_{Bn} is used as an argument in $v_{ms}(\theta)$ because the upstream plasma flow is anti-parallel to $\hat{\mathbf{n}}$. M_{ms} is defined as the flow speed divided by the group speed of the wave in the normal direction and is therefore dependent on θ_{Bn}. The Alfvén Mach number is usually defined in a different way. Both the slow and intermediate wave mode can only propagate along $\mathbf{B}$ and the Mach numbers would explode for θ_{Bn} close to 90°. Therefore the Alfvén Mach number in the NI frame is typically just defined as

$$M_A = \frac{|\mathbf{V}_u \cdot \hat{\mathbf{n}} - V_{sh}|}{v_A}, \tag{6.28}$$

and is therefore independent on θ_{Bn}. Both M_A and M_{ms} are commonly used in shock physics and the determination of the Mach numbers is reliant on accurate estimates of V_{sh} and $\hat{\mathbf{n}}$.

7. Ion acceleration at collisionless shocks

Shock waves are some of the most efficient particle accelerators in space. Shock waves around supernova remnants are believed to be the primary source of galactic cosmic rays. The cosmic rays are energetic charged particles and are mainly ions [Longair, 2011]. The spectrum of cosmic ray protons between energies of 10^9 and 10^{15} eV can be described by power-law distribution $\propto E^{-2.7}$. This universal spectrum is an important feature that gives crucial information about the source of the cosmic rays. Here we review the original proposed mechanism for accelerating cosmic rays and the current model of diffusive shock acceleration as a fundamental acceleration mechanism at shocks.

7.1 Fermi acceleration

An early model of how galactic cosmic rays are accelerated was proposed by [Fermi, 1949]. He suggested that the cosmic ray ions are accelerated in the interstellar space in the galaxy by "colliding" repeatedly with magnetic disturbances. A collision with the interstellar magnetic disturbances can be seen as a reflection off an obstacle, moving in a random direction with speed V. An ion with a speed much greater than V can undergo a head-on collision where it will gain energy or an overtaking collision where it loses energy, see Figure 7.1. The key to the acceleration mechanism is that head-on collisions are slightly more common since the relative speeds are greater. Therefore, the energy of an ion undergoing many such collisions will inevitably increase. Assuming the ion already has a high energy so that its speed approaches c, then the average gain in energy E per collision is

$$\frac{\Delta E}{E} \propto \left(\frac{V}{c}\right)^2 \tag{7.1}$$

Since the energy increase is proportional to $(V/c)^2$, this process is referred to as a *second order Fermi acceleration*. There are some problems with this mechanism to generate cosmic rays [Longair, 2011]. First, the speed of the interstellar magnetic disturbances is typically quite low (∼tens of km/s) and collisions very infrequent. This means that the acceleration is very slow and losses due to e.g. ionization in collision with the interstellar medium could be greater than the acceleration. Second, the second order Fermi process produces a power-law distribution function in the ion energy spectra but there is

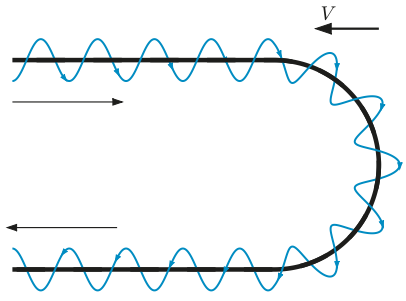

Figure 7.1. Sketch of the second-order Fermi acceleration process. A gyrating energetic ion impinges on a surface that is moving against the speed of the ion.

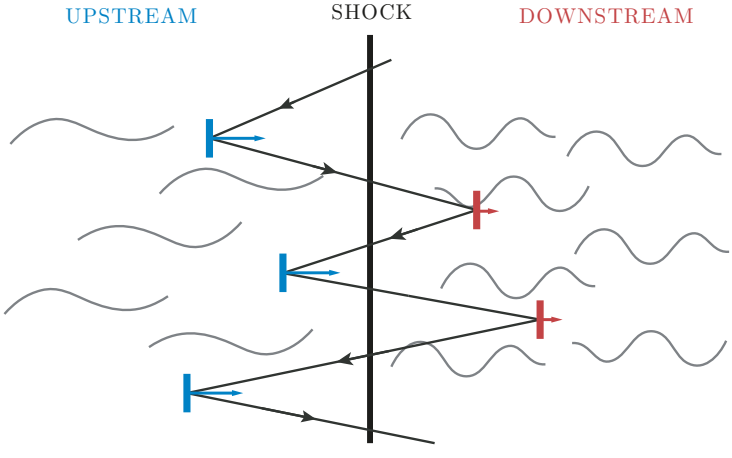

Figure 7.2. Sketch of the DSA process. An energetic ion is diffused on both sides of the shock. This leads to an energy increase over time.

no reason that this power law should universally be close to the value of -2.7 like for the cosmic rays. Another model of cosmic ray acceleration is clearly required.

7.2 Diffusive shock acceleration (DSA)

In the modern understanding of how cosmic rays are generated, ions are accelerated in collisionless shock waves around supernova remnants (SNRs). The process known as diffusive shock acceleration (DSA) [Axford et al., 1977, Krymskii, 1977, Bell, 1978, Blandford and Ostriker, 1978] is a stochastic process where ions gain energy by repeatedly crossing the shock, see Figure 7.2. Here we review the basic ingredients of this acceleration process.

Consider an energetic ion crossing from the downstream side of a shock to the upstream side. Since we're dealing with a strong shock wave, the upstream speed in the shock frame is V_u and the downstream speed is $V_d = V_u/4$ (see Section 5.3). In the downstream frame, the upstream speed is therefore $3V_u/4$,

toward the shock. The ion crosses from down- to upstream and in the upstream frame the energy of the ion is higher. Since the shock itself is non-relativistic and $V_u \ll c$ the ion kinetic energy in the upstream frame is

$$E' = E + \frac{3V_u}{4} p_n \tag{7.2}$$

where E is the ion kinetic energy in the downstream frame and the normal component of the momentum is

$$p_n = p\cos\theta \tag{7.3}$$

where θ is the angle of incidence of the ion to the shock normal. In the high-energy limit $E = pc$ and the fractional energy increase is

$$\frac{E' - E}{E} = \frac{3V_u}{4c}\cos\theta. \tag{7.4}$$

Because the fractional energy gain is proportional to V_u/c, DSA is referred to as a *first order Fermi acceleration* process. Since the ion has a random velocity in three dimensions, the probability of θ is proportional to $\sin\theta$. And since the probability of the ion encountering the shock is proportional to p_n and therefore proportional to $\cos\theta$. Therefore the average energy increase is

$$\left\langle \frac{E' - E}{E} \right\rangle = \frac{3V_u}{4c} \int_0^{\pi/2} 2\cos^2\theta \sin\theta \mathrm{d}\theta = \frac{V_u}{2c} \tag{7.5}$$

Now consider the same ion being scattered in the upstream frame, maintaining a constant energy E' in that frame. Now the ion crosses downstream again. However, in the upstream frame the downstream speed is $3V_u/4$ toward the shock, exactly the same situation as in the first shock crossing from down- to upstream. Therefore the ion again gains energy when switching frames. The average energy increase in one round-trip is

$$\beta \equiv \left\langle \frac{\Delta E}{E} \right\rangle = \frac{V_u}{c}. \tag{7.6}$$

This acceleration process is repeated until the high-energy ion escapes the shock region. In the model, we assume an infinite extent of the plasma both normal and tangential to the shock wave. Therefore, the only way for the ion to escape the region is to be convected by the downstream flow. In reality, the energy a ion can attain through DSA is limited by the size of the shock. In our model, the probability that the ion remains in the shock region each round trip is $P = 1 - V_u/c$ [Bell, 1978], where we have assumed that the speed of the high-energy ion is close to c.

Now we know, the average increase of energy for a high-energy ion crossing the shock and we know its probability to remain close the shock. If we have

many such ions undergoing DSA, the ions will tend to follow some distribution function. Consider a number of ions denoted by N_0. All these ions have a starting energy of E_0. After k number of back-and-forth crossings of the shock, the expected number of ions left is $N(E) = N_0 P^k$ and their expected energy is $E{=}E_0(1+\beta)^k$. We therefore get

$$\frac{\ln N/N_0}{\ln N/N_0} = \frac{\ln P}{\ln(1+\beta)}, \tag{7.7}$$

which leads to

$$N(E) = N_0 \left(\frac{\ln E}{\ln E_0}\right)^{\ln P/\ln(1+\beta)}, \tag{7.8}$$

which is a power-law distribution of particles. The particles with energy E remain in the shock region and can be accelerated further. So $N(E)$ is the number of particles with energy $\geq E$. The distribution function f is found from

$$N(E) = \int_E^\infty f(E)\mathrm{d}E. \tag{7.9}$$

This means that

$$f(E) \propto E^{\ln P/\ln(1+\beta)-1}. \tag{7.10}$$

Plugging in the values for P and β and using the first term in the Taylor expansion $\ln(1+x)\approx x$ gives

$$f(E) \propto E^{-2}. \tag{7.11}$$

This result is different from the original Fermi mechanism since it produces a universal power-law in the ion spectrum, as is observed in cosmic rays.

The above approach to DSA theory contains the basic physical process behind the acceleration of cosmic rays. The process of DSA is influenced by the presence of a magnetic field and its angle to the shock normal. The process also changes when the shock is weak or in the other end of the spectrum, when the shock itself is relativistic. The spectral slope for cosmic rays observed at the Earth is close to -2.7. The steeper slope of cosmic rays compared to DSA theory can be explained by losses during transport in the galaxy and escape from the shock that is not accounted for in the DSA model [Caprioli and Spitkovsky, 2014]. The energy conversion rate from kinetic energy of the shock to high-energy ions have been found in computer simulations [e.g. Caprioli and Spitkovsky, 2014] to be quite high ($\sim$20 %). Therefore, the accelerated ions will in turn influence the flow and induce turbulence up- and downstream, potentially increasing the rate of acceleration. This current theory of non-linear diffusive shock acceleration treats the shock and accelerated ions as a self-organizing system [Malkov and Drury, 2001].

7.3 The injection problem

In DSA, we often presume there is a population of already accelerated ions that are then further accelerated. The speed of the pre-accelerated ions must be much higher than the speed of the shock in order for them to cross the shock several times and not to be convected downstream. The question about how ions are first accelerated from the thermal population is known as the *injection problem*.

DSA has been observed to accelerate ions at the Earth's bow shock [e.g Ellison and Moebius, 1987, Kis et al., 2004]. However, due to the limited size of the bow shock, the maximum energy is limited by ions escaping the shock. Therefore, studies using spacecraft data from the Earth's bow shock are more suited to focus on the injection of ions. In a study using data from Cluster, Kis et al. [2013] found evidence of ion injection at Earth's quasi-parallel bow shock. The proposed mechanism is gyrosurfing acceleration when a SLAMS merge with a wave packet, which has trapped ions. In recent computer simulations Caprioli et al. [2015] show ions being reflected off a quasi-parallel shock. The shock is self-reforming, which makes the reflection efficiency unsteady. The magnetic field upstream of the shock is magnified and turned so that the local shock geometry becomes quasiperpendicular. This allows reflected ions to return to the shock and undergo several reflection, gaining energy each time. In Paper I and Paper IV, we study the mechanisms of ion injection at the Earth's bow shock and how it depends on shock conditions.

8. Shock non-stationarity

8.1 The non-stationary shock

We have seen that quasi-parallel shocks are extended and time-varying transitions. Quasi-perpendicular shock waves are on the other hand often considered sharp and stable and not changing with time unless the upstream conditions change. However, under certain conditions even a quasi-perpendicular shock can become non-stationary. This means that even under stable upstream conditions, the structure and motion of the shock becomes unsteady and changes with time. Shock non-stationarity is linked to the ion dynamics at the shock and are therefore on the time scale of the ion gyrofrequency and on the spatial scale of the ion gyroradius.

The first theoretical prediction of shock non-stationarity was made by Auer et al. [1962] and the first observations were made in a laboratory plasma by Morse et al. [1972]. Shock non-stationarity has been extensively studied in numerical simulations. Krasnoselskikh et al. [2002] showed theoretically and in simulations that above a critical nonlinear whistler Mach number, the nonlinear whistler wave that make up the shock ramp cannot stand in the flow anymore and the shock becomes intrinsically unstable. This critical nonlinear Mach number is a transition between stationarity and non-stationarity and has the expression

$$M_{nw} = \sqrt{\frac{m_i}{2m_e}} \cos\theta_{Bn}. \tag{8.1}$$

Shock non-stationarity may take many forms. The two main types of non-stationarity we will discuss here are *shock self-reformation* and *shock ripples*.

8.2 Self-reformation

A commonly observed feature of shocks in fully kinetic simulations is self-reformation of the shock front [e.g. Lembège and Savoini, 2002]. This is a process where a new shock front cyclically forms in the foot, upstream of the old front. The new shock front is convected in the downstream direction and eventually another shock front forms in front of that one. In a study using multi-spacecraft data from Cluster Lobzin et al. [2007] presented evidence for shock non-stationarity by observations of different magnetic structure of the shock for different spacecraft, as well as a time variability of reflected

ions with a period of the order of the ion gyroperiod. Sulaiman et al. [2015] presented evidence of high Mach number shocks undergoing self-reformation at Saturn's bow shock using Cassini data.

8.3 Shock ripples

An important kind of shock non-stationarity is rippling, which is a phenomenon where ion-kinetic waves, or ripples, move along the shock surface. These waves are commonly observed in fully kinetic and hybrid simulations of shocks. Winske and Quest [1988] first described of shock ripples in hybrid 2D simulations of a nearly perpendicular shock. Ripples have been shown to influence ion dynamics and acceleration processes of shocks [e.g. Yang et al., 2012, Hao et al., 2016]. In simulations, ripples have been shown to accelerate electrons to high energies [Umeda et al., 2009]. Lowe and Burgess [2003] in detail determined the dispersive properties of the ripples and found that they propagate along the magnetic field with phase speed close to the local Alfvén speed, and with a frequency of a few times the upstream ion cyclotron frequency. Also in 3D simulations, Burgess et al. [2016] found that the shock structure is dominated by a combination of fluctuations propagating along the magnetic field and in the direction of reflected ion gyration. At higher Mach number ($M_A = 5.5$) field-propagating ripples are the dominant feature. The first observations of shock ripples were made using Cluster data by Moullard et al. [2006] who exploits a slow and partial shock crossing to conclude that the shock is rippled. However, the observed dispersive properties of the ripples do not match the ion-kinetic scales reported in simulations. In Paper I and Paper II, we study shock ripples using MMS high-cadence measurements, which can resolve the kinetic scales of the ripples.

9. Outlook

In this thesis we have investigated structure and ion dynamics of quasi-parallel and quasi-perpendicular shock waves. The MMS spacecraft offer entirely new opportunities to study shock physics on kinetic scales. There are for instance many still unresolved questions about how ions are injected and accelerated at quasi-parallel shocks that MMS is very well suited to explore. Observations from MMS could also be further compared to large scale hybrid and fully kinetic simulations in two and three dimensions. Simulations can offer a more complete picture of structure of the shock and of how particles move. Spacecraft observations can be used to test and validate the predictions from simulations. There have been a few studies of how electrons are heated and energized at collisionless shock waves using MMS data [Oka et al., 2017, Chen et al., 2018], but there is still many questions MMS can help resolve. One such question is regarding the scale at which electrons are heated at quasi-perpendicular shocks and what role non-adiabatic processes play in the heating. A preliminary study of this, highlighting the capabilities of MMS has been done by Svensson [2018]. Finally, exciting new opportunities for shock studies in space are opening up with the recent launch of NASA's Parker Solar Probe and the planned launch of ESA's Solar Orbiter spacecraft. These missions will probe the plasma environment closer to the Sun than ever before. This will enable shock studies regarding e.g. interplanetary shock waves in different plasma conditions, early shock evolution, and the formation of solar energetic particles.

10. Summary of papers

10.1 Paper I

Title
Ion injection at Quasi-parallel Shocks Seen by the Cluster Spacecraft

Authors
A. Johlander, A. Vaivads, Yu. V. Khotyaintsev, A. Retinò, and I. Dandouras

Journal
Astrophysical Journal Letters

Details
Year: 2016, Volume: 817, Issue: 1

My contribution
I performed the data analysis and had the main responsibility for writing the paper.

In Paper I, we study ion acceleration at the Earth's quasi-parallel bow shock using Cluster data. We take advantage of the sub-spin-resolution ion data from the CIS-HIA instrument onboard Cluster 1 and 3 to get the highest possible time-resolution. We investigate in detail, how ions are accelerated and injected into DSA at a short large amplitude magnetic structure (SLAMS).

We find that solar wind ions are almost specularly reflected off the SLAMS. Gyration in the solar wind, with constant energy in the solar wind frame, leads to acceleration and an energy increase to 2-3 times the solar wind energy, see Figure 10.1. We also perform test particle simulations using field data from spacecraft measurements. In the simulation, solar wind ions with slightly lower energies are more likely to be reflected off the SLAMS while higher-energy ions are more likely to pass through the SLAMS and continue downstream. This is consistent with the observed ion distributions up- and downstream of the SLAMS. The acceleration of ions that are reflected off SLAMS provides a mechanism for explaining how upstream ions undergo initial acceleration and can be injected into diffusive shock acceleration.

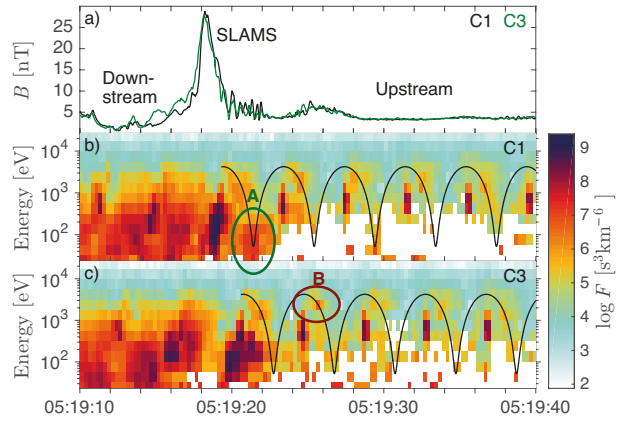

Figure 10.1. The SLAMS observed by C1 and C3. (a) Magnetic field amplitude for two spacecraft. (b)–(c) Ion phase-space density averaged over polar angle in sub-spin resolution. Two ion populations upstream of the SLAMS are circled and denoted by A and B. A: Reflected ions just upstream of the SLAMS. B: Ions with higher energy than the solar wind; these ions are seen by both spacecraft and farther upstream as well. The solid lines in (b-c) indicate constant energy in the solar wind frame.

10.2 Paper II

Title

Rippled Quasiperpendicular Shock Observed by the Magnetospheric Multiscale Spacecraft

Authors

A. Johlander, S. J. Schwartz, A. Vaivads, Yu. V. Khotyaintsev, I. Gingell, I. B. Peng, S. Markidis, et al.

Journal

Physical Review Letters

Details

Year: 2016, Volume: 117, Issue: 16

My contribution

I performed the data analysis and had the main responsibility for writing the paper.

In Paper II, we study the structure of the shock at a quasi-perpendicular bow shock crossing by MMS. Thanks to MMS high-cadence measurements, we present, for the first time, observations of ion distribution functions at ion kinetic scales at the bow shock.

At the time of the bow shock crossing, the four MMS spacecraft are closely spaced with inter-spacecraft distances of $\sim$25 km. Despite this, the four spacecraft observe rather different shock profiles. We also observe ion phase-space holes in the ion distribution, see Figure 10.2. We conclude that the differences between the spacecraft are due to the shock seemingly repeatedly moving up- and downstream across the spacecraft, i.e the shock is non-stationary. The phase-space holes are due to that the spacecraft go between observing the shocked downstream plasma and the counterstreaming beams of solar wind and reflected ions. With a detailed analysis of the four-spacecraft field and ion measurements, we find that the non-stationarity is in the form of shock ripples moving along the shock front. Quantitative analysis show that the ripples are moving close to the local Alfvén speed with a wavelength of a few ion inertial lengths, in good agreement with previous 2D hybrid simulations.

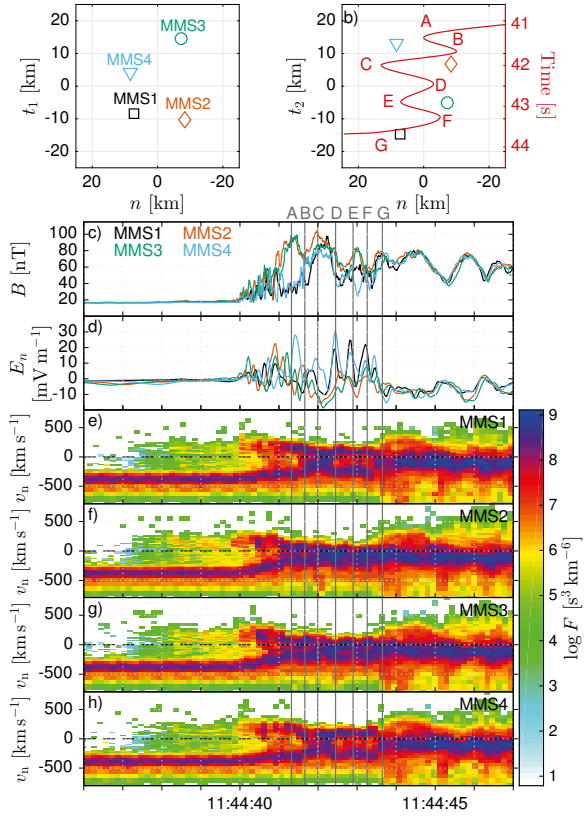

Figure 10.2. Four-spacecraft observations of electric, magnetic field, and ion distributions. (a),(b) Spacecraft positions. (b) The red line shows the apparent shock position along $\hat{\mathbf{n}}$ over time, the back and forth motion is due to the ripples. (c) Magnetic field magnitude. (d) Normal electric field. (e)–(h) Ion phase-space density as functions of the normal speed averaged over tangential velocities.

10.3 Paper III

Title

Shock Ripples Observed by the MMS spacecraft:
Ion Reflection and Dispersive Properties

Authors

A. Johlander, A. Vaivads, Y. V. Khotyaintsev, I. Gingell, S. J. Schwartz, B. L. Giles, R. B. Torbert, and C. T. Russell

Journal

Plasma Physics and Controlled Fusion

Details

Year: 2018, Volume: 60, Issue: 12

My contribution

I performed the data analysis and had the main responsibility for writing the paper.

In Paper III we study shock ripples using MMS data in greater detail than before, in particular related to dispersive properties of the ripples and what effect they have on ion reflection. The trajectory of MMS in the event presented here was very favorable for studies of shock non-stationarity since MMS skimmed the shock front for almost 1 minute and the more than 15 periods of ripples were observed.

During the event, we observe large amplitude fluctuation in the magnetic field and ion density. As before, we observe ion phase-space holes as the spacecraft repeatedly goes up- and downstream of the shock ramp. The shock is clearly non-stationary. Using four-spacecraft observations, we conclude that the non-stationarity is in the form of ripples. Due to the long encounter with the ripples with all four spacecraft, we can in detail determine dispersive properties of the ripples.

We find that the ripples propagate in the coplanarity plane with an angle to the shock surface of $\sim 40^{\circ}$ with a phase speed in the NI frame close to the local Alfvén speed. The frequency of the ripples is ~ 3 times the upstream ion gyrofrequency and the wavelength is ~ 5 times the upstream ion inertial length. Moreover the ripples are nearly linearly polarized with fluctuations mainly in the coplanarity plane, leading to an almost two-dimensional structure of the ripples. We compare the observations of the shock ripples with a numerical dispersion solver and find that the ripples resemble Alfvén waves generated by an ion temperature anisotropy. Finally, with the detailed four-spacecraft observations, we can map different plasma parameters as a function of phase

of the ripples and distance to the shock overshoot, see Figure 10.3. We find that the density of reflected ions is highly localized along the rippled shock. This means that ions are preferentially reflected in regions of the ripples with magnetic field stronger than the average overshoot field, while in the regions of lower magnetic field, ions penetrate the shock to the downstream region. This means that ripples may play an important role in ion heating and energization at shocks.

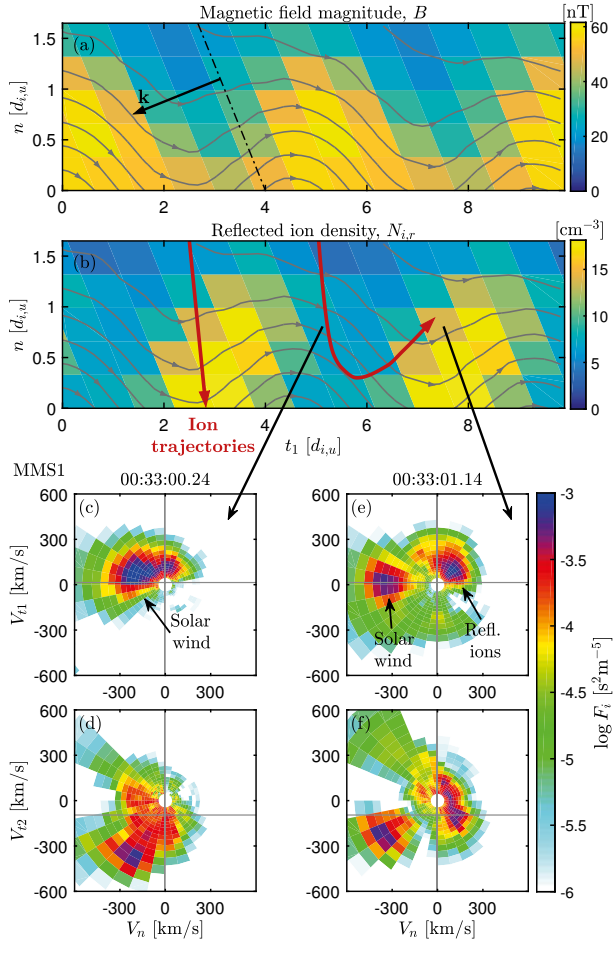

Figure 10.3. 2D histograms of the rippled shock compiled with data from all four spacecraft and representative ion distribution functions. (a) Magnetic field magnitude in the shock. Also shown are approximate field lines given from the magnetic field data. (b) Density of reflected ions. Two inferred ion trajectories for two incidence locations are shown as red arrows. (c)–(f) Projected ion distribution function, in two planes, for two times corresponding to different regions in the shock indicated by black arrows

10.4 Paper IV

Title

Conditions for Ion Acceleration at Collisionless Shock Waves

Authors

A. Johlander, A. Vaivads, Yu. V. Khotyaintsev, Damiano Caprioli, C. C. Haggerty, S. J. Schwartz

Status

Manuscript in preparation

My contribution

I performed the data analysis and had the main responsibility for writing the paper.

In Paper IV we study ion acceleration at the Earth's bow shock using MMS. The study is in part a statistical study that quantifies the ion acceleration efficiency dependence on upstream and shock conditions. The other part is a case study of one shock crossing with high acceleration efficiency where we discuss the effect of SLAMS on the thermal, suprathermal, and energetic ion populations.

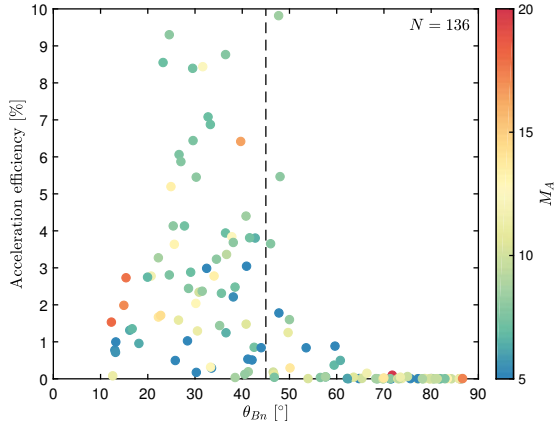

Figure 10.4. .

For the statistics, we investigate the conditions for ion acceleration using 136 crossings of the Earth's bow shock by the four MMS satellites. We determine bow shock parameters like Mach numbers and shock angle by using upstream solar wind monitor spacecraft through the OMNI database. Using MMS, we quantify ion acceleration efficiency of the shock and the depen-

dence on shock parameters. We find that quasi-parallel shocks are more efficient at accelerating ions with up to 10% of the energy density in energetic ions. Energetic ions are defined as having energies greater than 10 times the solar wind energy. Above a shock angle of $\sim 60^{\circ}$, essentially no energetic ions are observed in any of the events. We find that ion acceleration efficiency is significantly lower for low Mach number ($M_A < 6$) shocks while there is no Mach number dependence above this. We also find that ion acceleration is lower on the flanks of the bow shock than at the sub-solar point regardless of the Mach number.

Next, we in detail investigate one crossing of the quasi-parallel shock with a high acceleration efficiency. We find that SLAMS are important for the acceleration process. Solar wind ions are reflected off the SLAMS, which causes an initial acceleration. Furthermore, the highest densities of energetic ions are observed at the SLAMS rather than the shock itself. This is because the SLAMS trap backstreaming energetic ions and convect them back toward the shock, which is important for the acceleration process since this increases the time the high-energy ions spend close to the shock.

11. Sammanfatting på svenska

Den till synes tomma rymden mellan planeter och stjärnor är i själv verket inte alls tom utan består av plasma. Plasma är en gas av laddade partiklar och finns överallt i universum. Precis som i en vanlig gas kan det uppstå chockvågor i ett plasma. Sådana chockvågor finns till exempel runt stjärnor som har exploderat till supernovor men de finns också i vårt solsystem. I många rymdplasma är kollisioner mellan de laddade partiklarna mycket ovanliga. Ett sådant plasma kallas för *kollisionsfritt* och där styr de elektriska och magnetiska krafterna hur partiklarna rör sig. Det är vanligt att undersöka fysiken kring kollisionsfria chockvågor genom att studera dem med teleskop eller med stora datorsimuleringar. Ämnet för den här avhandlingen är att studera fysiken kring kollisionsfria chockvågor med hjälp av mätningar som görs av rymdfarkoster i omloppsbana kring jorden. Av särskilt intresse är hur strukturen av chockvågorna ser ut i detalj och hur det påverkar de positivt laddade jonerna som finns i plasmat.

Solen skickar hela tiden ut en mycket snabb vind av plasma i alla riktningar. När denna solvind stöter på ett hinder, som till exempel en planets magnetfält, uppstår det en chockvåg som plötsligt bromsar och värmer upp plasmat. Chockvågen som bildas är inte helt olik en våg framför en båt som rör sig genom vatten, därför kallas chockvågen framför en planet ofta för en *bogchock*. I den här avhandlingen använder vi data från de europeiska ESA-satelliterna *Cluster* samt de amerikanska NASA-satelliterna *MMS* när de flyger genom jordens bogchock. Vi använder på så sätt bogchocken som ett naturligt plasmalaboratorium för att testa modeller kring struktur och jondynamik vid chockvågor i rymdplasma.

I den första studien använder vi data från Cluster vid den *kvasiparallella* bogchocken där magnetfältet bildar en vinkel mindre än 45° med chockens normalvektor. Vi studerar hur joner accelereras vid starka magnetiska strukturer som kallas *SLAMS* (short large amplitude magnetic structures). Vi observerar att joner från solvinden kan reflekteras vid SLAMS och på så vis accelereras. Vi föreslår detta som ett sätt för joner att genomgå första steget av acceleration för att sedan accelereras ytterligare. I andra studien använder vi data från MMS vid den *kvasivinkelräta* bogchocken där magnetfältet bildar en vinkel större än 45° med chockens normalvektor. Med MMS kan vi för första gången se hur småskaliga ($\sim$100 km) *krusningar*, eller vågor, rör sig längst med ytan på chockvågen. I tredje studien följer vi upp krusningarna i chockvågor med ännu mer detaljerade observationer från MMS. Vi mäter med stor noggrannhet krusingarnas egenskaper och studerar hur de påverkar jonreflektion vid chockvågor. I fjärde studien genomför vi en statistisk studie med

MMS om hur effektiva chockvågor är på att accelerera joner, och hur effektiviteten beror på chockvågens olika parametrar. Vi finner att kvasiparallella chockvågor är mycket mer effektiva än kvasivinkelräta på att accelerera joner. Vi ser också att SLAMS vid kvasiparallella chockvågor kan hindra högenergiska joner från att ta sig uppströms och tar dem tillbaka till chocken, vilket potentiellt ökar accelerationseffektiviteten.

Acknowledgments

There are many people I would like to thank for making this thesis possible. First and foremost I would like to thank my advisor Andris Vaivads for always taking the time and for all the support, guidance, and superb explanations of plasma physics. A big thanks also goes to my co-supervisors: Yuri Khotyaintsev, Emiliya Yordanova, and Alessandro Retinò for all the help. I am grateful to Mats André for always asking hard questions. I would also like to thank Steven Schwartz at LASP for teaching me much of what I know about shock waves.

I am grateful to all the PhD students at IRF. Special thanks to Elin Eriksson for always being available to talk about science or anything else. To all the current PhD students: Fredrik, Konrad and Katerina, and the previous students: Elias, Cecilia, Oleg, Ilka, and Mika for the great company over the years. A big thanks also goes out to all the staff at IRF and the astronomy division in Uppsala. Thanks to my very first advisor at IRF, Anders Eriksson for introducing me to space physics, to Daniel Graham for sharing the office with me and answering all my stupid questions, and to Erik Johansson for organizing the weekly board game sessions.

I would like to thank all the people and organizations that made this thesis possible. Thanks to the instrument and scientific teams of MMS and Cluster for all the hard work on the data and for creating a great scientific community. Thanks also to IRF, Uppsala University, and the Swedish National Space Agency.

I would like to thank Dryck & Mat and Lilla Ego and my friends who brought me there. And last but not least, thanks to my parents, grandpa, and sister for always supporting me.

References

B. Abraham-Shrauner. Determination of magnetohydrodynamic shock normals. *J. Geophys. Res.*, 77:736, 1972. doi: 10.1029/JA077i004p00736.

P. L. Auer, H. Hurwitz, Jr., and R. W. Kilb. Large-Amplitude Magnetic Compression of a Collision-Free Plasma. II. Development of a Thermalized Plasma. *Physics of Fluids*, 5:298–316, Mar. 1962. doi: 10.1063/1.1706615.

W. I. Axford, E. Leer, and G. Skadron. The acceleration of cosmic rays by shock waves. *International Cosmic Ray Conference*, 11:132–137, 1977.

A. Balogh, C. M. Carr, M. H. Acuña, M. W. Dunlop, T. J. Beek, P. Brown, K.-H. Fornacon, E. Georgescu, K.-H. Glassmeier, J. Harris, G. Musmann, T. Oddy, and K. Schwingenschuh. The cluster magnetic field investigation: overview of in-flight performance and initial results. *Annales Geophysicae*, 19(10/12):1207–1217, 2001. doi: 10.5194/angeo-19-1207-2001. URL `https://www.ann-geophys.net/19/1207/2001/`.

A. R. Bell. The acceleration of cosmic rays in shock fronts. I. *Mon. Not. R. Astron. Soc.*, 182:147–156, Jan. 1978. doi: 10.1093/mnras/182.2.147.

R. D. Blandford and J. P. Ostriker. Particle acceleration by astrophysical shocks. *Astrophys. J. Lett.*, 221:L29–L32, Apr. 1978. doi: 10.1086/182658.

J. L. Burch, T. E. Moore, R. B. Torbert, and B. L. Giles. Magnetospheric Multiscale Overview and Science Objectives. *Space Sci. Rev.*, 199:5–21, Mar. 2016. doi: 10.1007/s11214-015-0164-9.

D. Burgess, P. Hellinger, I. Gingell, and P. M. Trávníček. Microstructure in two- and three-dimensional hybrid simulations of perpendicular collisionless shocks. *Journal of Plasma Physics*, 82(4):905820401, Aug. 2016. doi: 10.1017/S0022377816000660.

D. Caprioli and A. Spitkovsky. Simulations of Ion Acceleration at Non-relativistic Shocks. I. Acceleration Efficiency. *Astrophys. J.*, 783:91, Mar. 2014. doi: 10.1088/0004-637X/783/2/91.

D. Caprioli, A.-R. Pop, and A. Spitkovsky. Simulations and Theory of Ion Injection at Non-relativistic Collisionless Shocks. *Astrophys. J. Lett.*, 798:L28, Jan. 2015. doi: 10.1088/2041-8205/798/2/L28.

F. F. Chen and S. E. von Goeler. Introduction to Plasma Physics and Controlled Fusion Volume 1: Plasma Physics, Second Edition. *Physics Today*, 38:87, 1985. doi: 10.1063/1.2814568.

L.-J. Chen, S. Wang, L. B. Wilson, S. Schwartz, N. Bessho, T. Moore, D. Gershman, B. Giles, D. Malaspina, F. D. Wilder, R. E. Ergun, M. Hesse, H. Lai, C. Russell, R. Strangeway, R. B. Torbert, A. F.-Vinas, J. Burch, S. Lee, C. Pollock, J. Dorelli, W. Paterson, N. Ahmadi, K. Goodrich, B. Lavraud, O. Le Contel, Y. V. Khotyaintsev, P.-A. Lindqvist, S. Boardsen, H. Wei, A. Le, and L. Avanov. Electron bulk acceleration and thermalization at earth's quasiperpendicular bow shock. *Phys. Rev. Lett.*, 120:225101, May 2018. doi:

10.1103/PhysRevLett.120.225101. URL https://link.aps.org/doi/10.1103/PhysRevLett.120.225101.

F. De Hoffmann and E. Teller. Magneto-hydrodynamic shocks. *Phys. Rev.*, 80: 692–703, Nov 1950. doi: 10.1103/PhysRev.80.692. URL http://link.aps.org/doi/10.1103/PhysRev.80.692.

J. P. Edmiston and C. F. Kennel. A parametric survey of the first critical Mach number for a fast MHD shock. *Journal of Plasma Physics*, 32:429–441, Dec. 1984. doi: 10.1017/S002237780000218X.

D. C. Ellison and E. Moebius. Diffusive shock acceleration - Comparison of a unified shock model to bow shock observations. *Astrophysical Journal*, 318: 474–484, July 1987. doi: 10.1086/165384.

R. E. Ergun, S. Tucker, J. Westfall, K. A. Goodrich, D. M. Malaspina, D. Summers, J. Wallace, M. Karlsson, J. Mack, N. Brennan, B. Pyke, P. Withnell, R. Torbert, J. Macri, D. Rau, I. Dors, J. Needell, P.-A. Lindqvist, G. Olsson, and C. M. Cully. The Axial Double Probe and Fields Signal Processing for the MMS Mission. *Space Sci. Rev.*, 199:167–188, Mar. 2016. doi: 10.1007/s11214-014-0115-x.

C. P. Escoubet, C. T. Russell, and R. Schmidt. *The Cluster and PHOENIX missions*. 1997.

D. H. Fairfield. Average and unusual locations of the Earth's magnetopause and bow shock. *J. Geophys. Res.*, 76:6700, 1971. doi: 10.1029/JA076i028p06700.

M. H. Farris, S. M. Petrinec, and C. T. Russell. The thickness of the magnetosheath - Constraints on the polytropic index. *Geophys. Res. Lett.*, 18:1821–1824, Oct. 1991. doi: 10.1029/91GL02090.

E. Fermi. On the Origin of the Cosmic Radiation. *Physical Review*, 75:1169–1174, Apr. 1949. doi: 10.1103/PhysRev.75.1169.

V. Formisano, P. C. Hedgecock, G. Moreno, F. Palmiotto, and J. K. Chao. Solar wind interaction with the Earth's magnetic field: 2. Magnetohydrodynamic bow shock. *J. Geophys. Res.*, 78:3731, 1973. doi: 10.1029/JA078i019p03731.

J. T. Gosling and M. F. Thomsen. Specularly reflected ions, shock foot thicknesses, and shock velocity determinations in space. *J. Geophys. Res.*, 90:9893–9896, Oct. 1985. doi: 10.1029/JA090iA10p09893.

Y. Hao, Q. Lu, X. Gao, and S. Wang. Ion dynamics at a rippled quasi-parallel shock: 2d hybrid simulations. *The Astrophysical Journal*, 823(1):7, 2016. URL http://stacks.iop.org/0004-637X/823/i=1/a=7.

A. Johlander, S. J. Schwartz, A. Vaivads, Y. V. Khotyaintsev, I. Gingell, I. B. Peng, S. Markidis, P.-A. Lindqvist, R. E. Ergun, G. T. Marklund, F. Plaschke, W. Magnes, R. J. Strangeway, C. T. Russell, H. Wei, R. B. Torbert, W. R. Paterson, D. J. Gershman, J. C. Dorelli, L. A. Avanov, B. Lavraud, Y. Saito, B. L. Giles, C. J. Pollock, and J. L. Burch. Rippled quasiperpendicular shock observed by the magnetospheric multiscale spacecraft. *Phys. Rev. Lett.*, 117:165101, Oct 2016. doi: 10.1103/PhysRevLett.117.165101. URL http://link.aps.org/doi/10.1103/PhysRevLett.117.165101.

A. Johlander, A. Vaivads, Y. V. Khotyaintsev, A. Retinò, and I. Dandouras. Ion injection at Quasi-parallel Shocks Seen by the Cluster Spacecraft. *Astrophys. J. Lett.*, 817:L4, Jan. 2016. doi: 10.3847/2041-8205/817/1/L4.

A. Johlander, A. Vaivads, Y. V. Khotyaintsev, I. Gingell, S. J. Schwartz, B. L. Giles, R. B. Torbert, and C. T. Russell. Shock ripples observed by the mms spacecraft:

ion reflection and dispersive properties. *Plasma Physics and Controlled Fusion*, 60 (12):125006, 2018. doi: 10.1088/1361-6587/aae920.

J. H. King and N. E. Papitashvili. Solar wind spatial scales in and comparisons of hourly Wind and ACE plasma and magnetic field data. *Journal of Geophysical Research (Space Physics)*, 110:A02104, Feb. 2005. doi: 10.1029/2004JA010649.

A. Kis, M. Scholer, B. Klecker, E. Möbius, E. A. Lucek, H. Rème, J. M. Bosqued, L. M. Kistler, and H. Kucharek. Multi-spacecraft observations of diffuse ions upstream of Earth's bow shock. *Geophys. Res. Lett.*, 31:L20801, Oct. 2004. doi: 10.1029/2004GL020759.

A. Kis, O. Agapitov, V. Krasnoselskikh, Y. V. Khotyaintsev, I. Dandouras, I. Lemperger, and V. Wesztergom. Gyrosurfing Acceleration of Ions in Front of Earth's Quasi-parallel Bow Shock. *Astrophys. J. Lett.*, 771:4, July 2013. doi: 10.1088/0004-637X/771/1/4.

V. V. Krasnoselskikh, B. Lembège, P. Savoini, and V. V. Lobzin. Nonstationarity of strong collisionless quasiperpendicular shocks: Theory and full particle numerical simulations. *Physics of Plasmas*, 9:1192–1209, Apr. 2002. doi: 10.1063/1.1457465.

G. F. Krymskii. A regular mechanism for the acceleration of charged particles on the front of a shock wave. *Akademiia Nauk SSSR Doklady*, 234:1306–1308, June 1977.

B. Lembège and P. Savoini. Formation of reflected electron bursts by the nonstationarity and nonuniformity of a collisionless shock front. *Journal of Geophysical Research (Space Physics)*, 107:1037, Mar. 2002. doi: 10.1029/2001JA900128.

P.-A. Lindqvist, G. Olsson, R. B. Torbert, B. King, M. Granoff, D. Rau, G. Needell, S. Turco, I. Dors, P. Beckman, J. Macri, C. Frost, J. Salwen, A. Eriksson, L. Åhlén, Y. V. Khotyaintsev, J. Porter, K. Lappalainen, R. E. Ergun, W. Wermeer, and S. Tucker. The Spin-Plane Double Probe Electric Field Instrument for MMS. *Space Sci. Rev.*, 199:137–165, Mar. 2016. doi: 10.1007/s11214-014-0116-9.

V. V. Lobzin, V. V. Krasnoselskikh, J.-M. Bosqued, J.-L. Pinçon, S. J. Schwartz, and M. Dunlop. Nonstationarity and reformation of high-Mach-number quasiperpendicular shocks: Cluster observations. *Geophys. Res. Lett.*, 34:L05107, Mar. 2007. doi: 10.1029/2006GL029095.

M. S. Longair. *High Energy Astrophysics*. Feb. 2011.

R. E. Lowe and D. Burgess. The properties and causes of rippling in quasi-perpendicular collisionless shock fronts. *Annales Geophysicae*, 21:671–679, Mar. 2003. doi: 10.5194/angeo-21-671-2003.

M. A. Malkov and L. O. Drury. Nonlinear theory of diffusive acceleration of particles by shock waves. *Reports on Progress in Physics*, 64:429–481, Apr. 2001. doi: 10.1088/0034-4885/64/4/201.

G. Morlino and D. Caprioli. Strong evidence for hadron acceleration in Tycho's supernova remnant. *Astron. Astrophys.*, 538:A81, Feb. 2012. doi: 10.1051/0004-6361/201117855.

D. L. Morse, W. W. Destler, and P. L. Auer. Nonstationary Behavior of Collisionless Shocks. *Phys. Rev. Lett.*, 28:13–16, Jan. 1972. doi: 10.1103/PhysRevLett.28.13.

O. Moullard, D. Burgess, T. S. Horbury, and E. A. Lucek. Ripples observed on the surface of the Earth's quasi-perpendicular bow shock. *J. Geophys. Res. (Space*

Physics), 111:A09113, Sept. 2006. doi: 10.1029/2005JA011594.

M. Oka, L. B. W. III, T. D. Phan, A. J. Hull, T. Amano, M. Hoshino, M. R. Argall, O. L. Contel, O. Agapitov, D. J. Gershman, Y. V. Khotyaintsev, J. L. Burch, R. B. Torbert, C. Pollock, J. C. Dorelli, B. L. Giles, T. E. Moore, Y. Saito, L. A. Avanov, W. Paterson, R. E. Ergun, R. J. Strangeway, C. T. Russell, and P. A. Lindqvist. Electron scattering by high-frequency whistler waves at earth's bow shock. *The Astrophysical Journal Letters*, 842(2):L11, 2017. URL `http://stacks.iop.org/2041-8205/842/i=2/a=L11`.

E. N. Parker. Dynamics of the Interplanetary Gas and Magnetic Fields. *Astrophys. J.*, 128:664, Nov. 1958. doi: 10.1086/146579.

G. Paschmann, N. Sckopke, J. R. Asbridge, S. J. Bame, and J. T. Gosling. Energization of solar wind ions by reflection from the earth's bow shock. *J. Geophys. Res.*, 85:4689–4693, Sept. 1980. doi: 10.1029/JA085iA09p04689.

C. Pollock, T. Moore, A. Jacques, J. Burch, U. Gliese, Y. Saito, T. Omoto, L. Avanov, A. Barrie, V. Coffey, et al. Fast Plasma Investigation for Magnetospheric Multiscale. *Space Sci. Rev.*, 199:331–406, Mar. 2016. doi: 10.1007/s11214-016-0245-4.

H. Rème, C. Aoustin, J. M. Bosqued, I. Dandouras, B. Lavraud, J. A. Sauvaud, A. Barthe, J. Bouyssou, T. Camus, O. Coeur-Joly, A. Cros, and et al. First multispacecraft ion measurements in and near the earth's magnetosphere with the identical cluster ion spectrometry (cis) experiment. *Annales Geophysicae*, 19 (10/12):1303–1354, 2001. doi: 10.5194/angeo-19-1303-2001. URL `https://www.ann-geophys.net/19/1303/2001/`.

S. P. Reynolds. Supernova Remnants at High Energy. *Annu. Rev. Astron. Astrophys.*, 46:89–126, Sept. 2008. doi: 10.1146/annurev.astro.46.060407.145237.

C. T. Russell, B. J. Anderson, W. Baumjohann, K. R. Bromund, D. Dearborn, D. Fischer, G. Le, H. K. Leinweber, D. Leneman, W. Magnes, J. D. Means, M. B. Moldwin, R. Nakamura, D. Pierce, F. Plaschke, K. M. Rowe, J. A. Slavin, R. J. Strangeway, R. Torbert, C. Hagen, I. Jernej, A. Valavanoglou, and I. Richter. The Magnetospheric Multiscale Magnetometers. *Space Sci. Rev.*, 199:189–256, Mar. 2016. doi: 10.1007/s11214-014-0057-3.

S. J. Schwartz. Shock and Discontinuity Normals, Mach Numbers, and Related Parameters. *ISSI Scientific Reports Series*, 1:249–270, 1998.

S. J. Schwartz and D. Burgess. Quasi-parallel shocks - A patchwork of three-dimensional structures. *Geophys. Res. Lett.*, 18:373–376, Mar. 1991. doi: 10.1029/91GL00138.

S. J. Schwartz, M. F. Thomsen, and J. T. Gosling. Ions upstream of the earth's bow shock - A theoretical comparison of alternative source populations. *J. Geophys. Res.*, 88:2039–2047, Mar. 1983. doi: 10.1029/JA088iA03p02039.

J. A. Slavin and R. E. Holzer. Solar wind flow about the terrestrial planets. I - Modeling bow shock position and shape. *J. Geophys. Res.*, 86:11401–11418, Dec. 1981. doi: 10.1029/JA086iA13p11401.

E. J. Smith and M. E. Burton. Shock analysis - Three useful new relations. *J. Geophys. Res.*, 93:2730–2734, Apr. 1988. doi: 10.1029/JA093iA04p02730.

A. H. Sulaiman, A. Masters, M. K. Dougherty, D. Burgess, M. Fujimoto, and G. B. Hospodarsky. Quasiperpendicular High Mach Number Shocks. *Phys. Rev. Lett.*, 115(12):125001, Sept. 2015. doi: 10.1103/PhysRevLett.115.125001.

M. Svensson. Electron heating in collisionless shocks observed by the MMS spacecraft. Master's thesis, Luleå University of Technology, Space Technology, 2018. URL http://urn.kb.se/resolve?urn=urn:nbn:se:ltu:diva-67892.

D. G. Swanson. Plasma waves (2nd edition). *Plasma Physics and Controlled Fusion*, 45(6):1069, 2003. URL http://stacks.iop.org/0741-3335/45/i=6/a=701.

R. B. Torbert, C. T. Russell, W. Magnes, R. E. Ergun, P.-A. Lindqvist, O. LeContel, H. Vaith, J. Macri, S. Myers, D. Rau, J. Needell, B. King, M. Granoff, M. Chutter, I. Dors, G. Olsson, Y. V. Khotyaintsev, A. Eriksson, C. A. Kletzing, S. Bounds, B. Anderson, W. Baumjohann, M. Steller, K. Bromund, G. Le, R. Nakamura, R. J. Strangeway, H. K. Leinweber, S. Tucker, J. Westfall, D. Fischer, F. Plaschke, J. Porter, and K. Lappalainen. The FIELDS Instrument Suite on MMS: Scientific Objectives, Measurements, and Data Products. *Space Sci. Rev.*, 199:105–135, Mar. 2016. doi: 10.1007/s11214-014-0109-8.

B. T. Tsurutani and R. G. Stone. Collisionless shocks in the heliosphere: Reviews of current research. *Washington DC American Geophysical Union Geophysical Monograph Series*, 35, 1985.

T. Umeda, M. Yamao, and R. Yamazaki. Electron Acceleration at a Low Mach Number Perpendicular Collisionless Shock. *Astrophys. J.*, 695:574–579, Apr. 2009. doi: 10.1088/0004-637X/695/1/574.

A. Vaivads, A. Retinò, and M. André. Magnetic reconnection in space plasma. *Plasma Physics and Controlled Fusion*, 51:124016, Dec. 2009. doi: 10.1088/0741-3335/51/12/124016.

J. Vogt, S. Haaland, and G. Paschmann. Accuracy of multi-point boundary crossing time analysis. *Annales Geophysicae*, 29(12):2239–2252, 2011. doi: 10.5194/angeo-29-2239-2011. URL https://www.ann-geophys.net/29/2239/2011/.

D. Winske and K. B. Quest. Magnetic field and density fluctuations at perpendicular supercritical collisionless shocks. *J. Geophys. Res.*, 93:9681–9693, Sept. 1988. doi: 10.1029/JA093iA09p09681.

Z. W. Yang, B. Lembège, and Q. M. Lu. Impact of the rippling of a perpendicular shock front on ion dynamics. *J. Geophys. Res. (Space Physics)*, 117:A07222, July 2012. doi: 10.1029/2011JA017211.

Acta Universitatis Upsaliensis

Digital Comprehensive Summaries of Uppsala Dissertations from the Faculty of Science and Technology 1750

Editor: The Dean of the Faculty of Science and Technology

A doctoral dissertation from the Faculty of Science and Technology, Uppsala University, is usually a summary of a number of papers. A few copies of the complete dissertation are kept at major Swedish research libraries, while the summary alone is distributed internationally through the series Digital Comprehensive Summaries of Uppsala Dissertations from the Faculty of Science and Technology. (Prior to January, 2005, the series was published under the title "Comprehensive Summaries of Uppsala Dissertations from the Faculty of Science and Technology".)

Distribution: publications.uu.se
urn:nbn:se:uu:diva-368091

ACTA
UNIVERSITATIS
UPSALIENSIS
UPPSALA
2019